minerals

MDPI

Article

Studying the Stability of the K/Ar Isotopic System of Phlogopites in Conditions of High T, P: $^{40}Ar/^{39}Ar$ Dating, Laboratory Experiment, Numerical Simulation

Denis Yudin [1], Nikolay Murzintsev [1], Alexey Travin [1,2,*], Taisiya Alifirova [1,3], Egor Zhimulev [1] and Sofya Novikova [1]

[1] V.S. Sobolev Institute of Geology and Mineralogy, Siberian Branch of the Russian Academyof Sciences, 3 Academician Koptyug ave., 630090 Novosibirsk, Russia; dsyudin@gmail.com (D.Y.); murzintsevng@gmail.com (N.M.); taa@igm.nsc.ru (T.A.); ezhimulev@igm.nsc.ru (E.Z.); sa_novikova@inbox.ru (S.N.)
[2] Faculty of Geology and Geography, National Research Tomsk State University, 634050 Tomsk, Russia
[3] Department of Lithospheric Research, University of Vienna, Althanstraße 14/UZA2, 1090 Vienna, Austria
* Correspondence: travin@igm.nsc.ru

Abstract: Typically, $^{40}Ar/^{39}Ar$ dating of phlogopites from deep-seated xenoliths of kimberlite pipes produces estimates that suggest much older ages than those when these pipes were intruded. High-pressure (3 GPa) laboratory experiments enabled the authors to explore the behaviour of argon in the phlogopite structure under the conditions that correspond to the mantle, at the temperatures (from 700 to 1000 °C), far exceeding closure temperature of the K/Ar isotopic system. "Volume diffusion" remains foremost for describing the mobility of argon in phlogopite at high pressures. The mantle material age can be estimated through the dating of the phlogopites from deep-seated xenoliths of kimberlites, employing the $^{40}Ar/^{39}Ar$ method, subject to correction for a partial loss of radiogenic ^{40}Ar when xenolith moves upwards to the Earth's surface. The obtained data served as the basis for proposing the behaviour model of the K/Ar isotopic system of minerals in conditions of great depths (lower crust, mantle), and when transporting xenoliths in the kimberlite melt.

Keywords: kimberlite pipes; mantle xenoliths; $^{40}Ar/^{39}Ar$ dating; laboratory experiments; numerical modelling

Citation: Yudin, D.; Murzintsev, N.; Travin, A.; Alifirova, T.; Zhimulev, E.; Novikova, S. Studying the Stability of the K/Ar Isotopic System of Phlogopites in Conditions of High T, P: $^{40}Ar/^{39}Ar$ Dating, Laboratory Experiment, Numerical Simulation. *Minerals* **2021**, *11*, 192. https://doi.org/10.3390/min11020192

Academic Editors: Alexandre V. Andronikov and David Phillips

Received: 24 October 2020
Accepted: 8 February 2021
Published: 12 February 2021

1. Introduction

The mantle is the Earth's shell, which is the most extensive in volume. However, we know little about it since the information is not readily accessible. Kimberlite melts, which entrap the material of the lithospheric mantle and ancient cratons while rising to the surface, remain a principal source of information on the Mantle structure and evolution. Currently, kimberlite bodies are found on all continents, where ancient platforms are known. They constitute a heterogeneous mixture of restitic, protomagmatic, xenogenic, and late-magmatic mineral parageneses. Determining the age of intrusion of kimberlites and the age of formation of entrapped by them deep-seated xenoliths is of great importance for tracing the evolution of the kimberlite melt from its origination to the ascent to the Earth's surface. The economic value of some kimberlite pipes, as motherlodes of diamonds, also increases the importance of age data, allowing diamond prospecting problems to be formulated more clearly.

Dating of kimberlites can be performed based on the U/Pb method for determining age by perovskite, and based on the $^{40}Ar/^{39}Ar$ and Rb/Sr method for determining age by phlogopite. $^{40}Ar/^{39}Ar$ dating method is also the most readily available method for acquiring information about the mantle material age. Dating of xenoliths entrapped by kimberlites, can be performed using the $^{40}Ar/^{39}Ar$ method for determining age by

phlogopite, because of phlogopite is quite common in the upper mantle rocks. As compared to the Rb/Sr isochronal method, the $^{40}Ar/^{39}Ar$ method, according to which only one Potassium-containing mineral phase is required, offers an advantage since it employs the spectrum of ages that makes it possible to reconstruct the thermal history of rocks formed in a complex manner. Reliability of data, obtained using the $^{40}Ar/^{39}Ar$ method, is usually defined by internal criteria of the method accuracy (isochronal regression, presence of plateaux in the spectrum, etc.) and external: by comparing with geological data, dating results obtained using other isotopic methods. To date, there are numerous works devoted to $^{40}Ar/^{39}Ar$ dating of phlogopites from kimberlites [1–10] and others.

In the interpretation of isotopic dating results, the concepts of stability in isotopic systems are of fundamental importance. Research studies of the mechanisms of argon diffusion with an evaluation of kinetic parameters of mobility (activation energy, frequency factor) are based on the experiments on stepped annealing in a vacuum [11–16], experiments, where laser heating is used [17–19], laboratory hydrothermal experiments.

Conditions for conducting laboratory hydrothermal experiments are selected to be as close to natural ones as possible, ensuring stability in the crystal structure of a mineral. Hodges presents one of the most complete overviews of the results of laboratory experiments on frequently used mineral-geochronometers, including phlogopite [20]. Lee and Aldama [21] offered a model of argon mobility, where both volume diffusion migration through lattice, and short path migration (through linear defects in the mineral structure) are presumed. At temperatures above 800 °C, a volume diffusion mechanism therewith predominates, below 500 °C a short path migration prevails.

It is worthy of note that if in crustal conditions, the effect of pressure on argon mobility, which implies that the P*Va term (P—pressure, Va—activation volume) is added to activation energy Ea, is minor, in conditions of considerable (mantle) depths, it may become significant. Thus, Harrison and co-authors had carried out hydrothermal experiments at high pressure (14 kbar) with biotite [22], muscovite (10 kbar) [23], based on which 14 cm^3/mol estimates of activation volume were obtained. This value should lead to substantial changes in argon mobility in the mantle conditions [24].

Closure temperature of the K/Ar isotopic system in phlogopite is known to be about 400 °C [20], while the estimated mantle temperature at around 100 km, at 30 kbar pressure, is ~1000 °C [25–28], what, at first glance, would seem a problem for potential accumulation of radiogenic ^{40}Ar in the phlogopite structure. However, $^{40}Ar/^{39}Ar$ examination of phlogopites from deep-seated xenoliths of kimberlites often produces complex age spectra with the values substantially exceeding the age of intrusion of kimberlite pipes [7,9,10,29], which is difficult to explain by the mere effect of pressure on argon mobility at depth. It is common to explain such data by contamination of a mineral-geochronometer with "excess" ^{40}Ar [29–32].

The problem of retaining argon in the structure of phlogopites at depth and at the temperatures, exceeding closure temperature of the K/Ar isotopic system in phlogopite, was considered in the work of Foland [33]. It has been known that Ar is more soluble in micas as compared to other mantle minerals [33–36]. Hence, with no other "sinks", argon will enter the phlogopite structure, rather than a denser lattice of olivine, garnet, pyroxenes. The situation can be considered in terms of the model, suggested by the example of high-pressure metamorphic complexes [37]. Exchange of radiogenic argon between phlogopite and environment occurs through the inter-grain space, characterised by a relatively increased mobility of argon and limited capacity. Argon migrates towards the nearest potential "sinks". In the mantle, only adjacent phlogopite grains represent such "sinks". In this case, radiogenic argon is efficiently accumulated in phlogopite grains, which provides a way of acquiring geologically significant $^{40}Ar/^{39}Ar$ dating results for phlogopites from xenoliths of kimberlites [38]. Radiogenic argon therewith is accumulated in phlogopite in line with the radioactive decay equation minus the percentage of argon, remaining within the inter-grain space. Taking the above-said into account, migration

of radiogenic ^{40}Ar from phlogopite is defined by the ratio between the inter-grain space volume and the phlogopite volume.

Our article attempts to comprehend the phlogopite capability for accumulating radiogenic ^{40}Ar at great (mantle) depths in conditions of high T-P, utilizing two approaches: (a) $^{40}Ar/^{39}Ar$ examination of phlogopites of mantle origin from diamond-containing kimberlite pipes; (b) high-pressure laboratory experiments, conducted to identify the mechanisms controlling the mobility of argon isotopes at high T-P; (c) numerical simulation of migration of argon isotopes at high T-P based on the regularities, established in laboratory experiments, and the above-suggested model; comparison between the obtained results and $^{40}Ar/^{39}Ar$ dating of phlogopites from deep-seated xenoliths.

2. Laboratory Experiment

Morphology, composition, and structural features of phlogopites from xenoliths of kimberlites, and phlogopites prior to and after high-pressure experiments were examined in the Centre of shared use of research equipment for multi-component and isotope studies of the Siberian Branch of the Russian Academy of Sciences (SB RAS MIS RE CSU) with the use of scanning electronic microscopy (electronic microscope MIRA3 with the system of microanalysis, TESCAN, Brno, the Czech Republic), electron probe microanalysis with electron probe (microanalyzer JXA-8100, JEOL, Tokyo, Japan), infrared spectroscopy (Fourier-spectrometer VERTEX 70 FT IR of the Bruker corporation, Karlsruhe, Germany) and X-ray structure analysis (X-ray diffractometer DRON-4, Joint Stock Company «Bourevestnik», Sankt-Petersberg, Russia).

Isotopic composition of argon of phlogopites from xenoliths of kimberlites, and phlogopites prior to and after high-pressure laboratory experiments was measured in SB RAS MIS RE CSU. Weighed amount of phlogopites together with weighed amount of biotite MSA-11 (DSS No.129-88), used as a monitor, were wrapped in the aluminium foil, placed into a quartz vessel and were sealed up after pumping air therefrom. Biotite MSA-11, prepared by the All-Russian scientific-research institute of mineral resources named after N.M. Fedorovsky in 1988 as a standard K/Ar specimen, was certified as the $^{40}Ar/^{39}Ar$ monitor using international standard specimens of muscovite Bern 4m, biotite LP-6 [39]. The mean value of calibration results, amounting to 311.0 $\pm$ 1.5 Ma, is assumed to be the integral age of biotite MSA-11. The procedure is noteworthy for the exposure of quartz vessels with specimens to radiation in a water-cooled channel of the research reactor facility at the Tomsk State Polytechnic University (Tomsk). With exposure to radiation in such conditions, vessels with specimens are heated to not more than 100 °C. Gradient of neutron current did not surpass 0.5% in the specimen size. Stepped heating experiments were conducted in a quartz reactor with external heat-up furnace. ^{40}Ar blank run (10 min at 1200 °C) provided results not exceeding 5×10^{-10} cm^3 STP. ZrAl SAES-getters were employed to clean argon. Isotopic composition of argon was measured by multi-collector mass-spectrometer Argus of the GV-Instruments company (England).

The high-pressure experiments were performed using a multi-anvil apparatus of "split sphere" type (BARS) at V.S. Sobolev Institute of Geology and Mineralogy of the Siberian Branch of Russian Academy of Sciences. The studies employed high-pressure cell (HPC) made of the mixture of refractory oxides ZrO_2 and CaO[40]. HPC is a prism 23 mm high, 20.5 mm wide with truncated edges. Parallel to the 4th order axis, there is an opening, into which a heater is inserted. HPC heating system is comprised of a cylinder-shaped thin-walled graphite heater, graphite covers installed along heater edges, Mo- disks, Mo- current leads. A bushing made of MgO with the examined specimen was mounted immediately in the graphite heater. Reaction volume was assembled as follows: cut bands of two phlogopites at different ages were placed into the platinum capsule (capsule sizes: outside/inside diameter 6/5 mm, height 10 mm), then the capsule was closed with a platinum cover and mounted in the MgO bushing. The bushing faces were closed with pellets, fabricated from MgO as well. Accuracy of measuring temperature in the experiments amounted to $\pm$25 °C, pressure-$\pm$0.2 GPa. Specimens were cooled by

quenching, namely, cutting-off the heater current with no pressure release. Quenching time was 2–3 s. Pressure was determined by calibration curve, constructed at the room temperature according to transitions between phases in PbSe and Bi standard substances. Temperature was estimated by calibration curve, expressing the dependence of the heater current power on PtRh 30/6 thermocouple readings. Further details of the experimental procedures are described in [41,42].

3. Results

3.1. Results of $^{40}Ar/^{39}Ar$ Dating of Phlogopite of the Mantle Xenoliths

Four mantle xenoliths of pyroxenites from diamond-bearing kimberlite Mir and Udachnaya–Vostochnaya pipes were selected for examination. The estimated age of pipes intrusion is 360−382 Ma [29,43,44]. Phlogopite therein is represented by large plates (M4/01—1−1.5 mm; M5/01—up to 3 mm; M31/01—up to 1 mm; UV300/09—up to 6 mm), fills micro-cracks up to 1mm thick and exists in the form of fine grains (50−200 μm) in reaction garnet rims (Figure 1). According to [45], large plates of phlogopite in xenoliths of pyroxenites are in a structural equilibrium condition with respect to other minerals of these rocks. Chemical composition of such phlogopites is in compliance with primarily metasomatic origin. They are considered to be associated with the processes of ancient enrichment of the continental lithosphere [46]. Within the Siberian craton, several stages of mantle metasomatism [47,48] are evident. One of the earliest stages had developed in the slowly cooled Archaean lithosphere due to ingress of metasomatic potassium-, REE- and phosphorus-rich fluids. Among minerals, there are phlogopite, sulphides, Cr-spinel, apatite, graphite. One of late-stage metasomatic events is considered as a treatment of the continental lithospheric mantle with oxidized astenospheric fluids, prior to developing kimberlite seats in the upper mantle. Reaction rims around pyroxenes and garnet seem to appear at this stage.

For $^{40}Ar/^{39}Ar$ dating, there had been selected large plates of a uniformly composed phlogopite, that correspond to the early metasomatic stage (Figure 1). There had been obtained age spectra (Table 1, Figure 2), in which, after moving upwards in the low-temperature section, either mini-plateau of two stages (specimens M-04/01, UV-300/09), or individual stages are seen with extremely high age values, which for specimens M4/01, M5/01 and UV300/09 amounted to 2568 ± 18, 2430 ± 17 and 2336 ± 16 Ma, respectively (Figure 2). The age spectrum of phlogopite M31/01 in a high-temperature section has a prominent mini-plateau aged 2288 ± 16 Ma. These age estimates correspond to the estimates of time, when the material from the mantle entered the crust of superposed fold belts of microcontinents (2.5−2.3 billion years) [49], that subsequently became the parts of the Siberian craton; they are in line with reformation processes in the mantle, and are likely to indicate the time of a major metasomatic event.

Thus, it can be inferred that despite being in the high-temperature mantle conditions for a long time, and being transported later to the surface in the kimberlite melt, the K/Ar isotopic system of phlogopite from xenoliths of pyroxenites retained all accumulated radiogenic (or excess) ^{40}Ar corrected for ^{40}Ar released due to volume diffusion.

When selecting the conditions for experimental modelling of phlogopite's staying in the mantle conditions, to identify the mechanisms that regulate mobility of argon isotopes, the authors were guided by the estimates of PT parameters of forming deep-seated xenoliths, from which the examined phlogopite was chosen (Table 2). Laboratory experiments were carried out, utilising two types of phlogopite—aged 8.5 Ma from the Kuhi-Lal field (Tajikistan, SW Pamir) rocks and aged 1872 Ma from magnesial skarns of the Aldanian shield. Bands of variously aged phlogopites were packed together so as not only to study the losses of radiogenic argon in the mineral lattice, but also to verify the potential for its migration from one mineral to another. There were four conducted experiments (T = 800, 850, 900 and 1000 °C) at 3 GPa pressure and 2 h long, and four laboratory experiments (T = 700, 800, 900 and 1000 °C) at 3 GPa pressure, 72 h long.

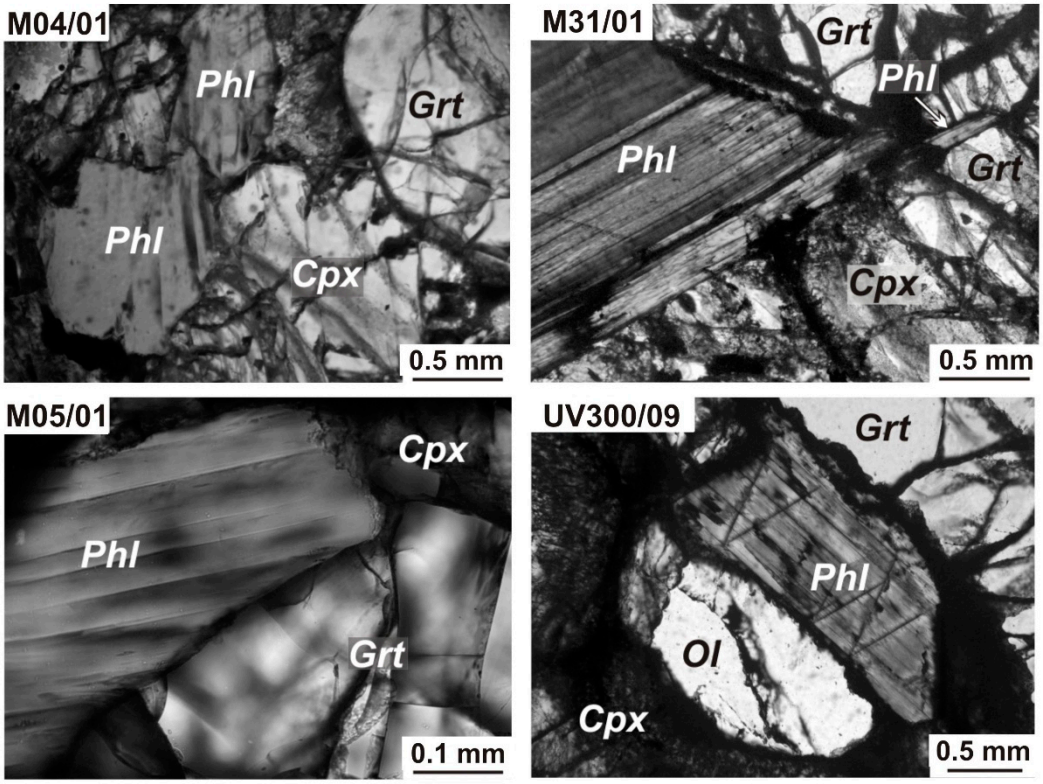

Figure 1. Morphology of the phlogopite from the studied xenoliths. Cpx—clinopyroxene, Grt—garnet, Ol—olivine, Phl—phlogopite.

Table 1. Results of $^{40}Ar/^{39}Ar$ dating of phlogopite samples from deep xenoliths of the Mir (Samples M4/01, M5/01, M31/01) and the Udachnaya–Vostochnaya (Sample UV300/09) kimberlite pipes.

T^0C	t (min)	^{40}Ar, 10^{-9} cm^3 STP	$^{40}Ar/^{39}Ar$	±1σ	$^{38}Ar/^{39}Ar$	±1σ	$^{37}Ar/^{39}Ar$	±1σ	$^{36}Ar/^{39}Ar$	±1σ	Ca/K	$\sum^{39}Ar$ (%)	Age, Ma	±1σ
M4/01 phlogopite (0.89 mg), J = 0.00465 ± 0.000057; Total Fusion Age (TFA) = 2404 ± 17 Ma														
500	10	3.56	257.26	33.76	0.0061	0.0499	0.500	0.6606	0.6720	0.1188	1.798	1.0	435.4	163.3
750	10	47.03	351.06	3.46	0.0729	0.0086	0.186	0.1020	0.1983	0.0089	0.669	11.1	1549.1	18.7
900	10	123.05	590.64	2.84	0.0330	0.0059	0.080	0.0559	0.0384	0.0046	0.286	26.8	2357.3	17.6
1000	10	135.97	627.21	1.91	0.0108	0.0021	0.108	0.0216	0.0453	0.0037	0.389	43.1	2434.1	17.0
1070	10	127.95	657.52	3.85	0.0475	0.0069	0.0701	0.0342	0.0962	0.00867	0.252	57.7	2467.0	19.1
1100	10	270.49	692.55	2.76	0.0194	0.0039	0.0434	0.0176	0.0349	0.00202	0.156	87.1	2577.1	17.7
1130	6	117.06	682.01	8.24	0.0498	0.0059	0.0012	0.0456	0.0397	0.0063	0.0043	100	2553.0	23.8
M5/01 phlogopite (0.74 mg), J = 0.00463 ± 0.000056; TFA = 2354 ± 17 Ma														
650	10	15.80	406.69	13.00	0.0816	0.0170	0.450	0.2223	0.1060	0.0323	1.620	5.1	1817.1	48.7
800	10	61.34	567.22	4.48	0.0018	0.0122	0.091	0.0577	0.0320	0.0150	0.326	19.3	2302.1	21.4
900	10	75.90	592.18	4.02	0.0282	0.0101	0.209	0.0552	0.0981	0.0051	0.753	36.2	2314.7	18.4
1000	10	67.17	608.56	7.21	0.0484	0.0136	0.082	0.0838	0.1039	0.0121	0.296	50.7	2348.4	23.6
1130	6	240.21	639.59	2.36	0.04	0.0028	0.115	0.0265	0.0849	0.0029	0.413	100	2429.8	17.0
M31/01 phlogopite (12.84 mg), J = 0.004611 ± 0.000056; TFA = 2099 ± 15 Ma														
500	10	9.65	232.22	9.02	0.1778	0.0298	0.816	0.0641	0.4849	0.0398	2.936	0.2	619.9	64.7
600	10	19.83	349.94	12.30	0.1836	0.0233	2.477	0.1171	0.5846	0.0282	8.917	0.5	1077.3	39.9
700	10	47.46	298.51	1.59	0.0601	0.0089	0.405	0.0222	0.1428	0.0083	1.459	1.3	1407.5	16.0

Table 1. *Cont.*

T^{0}C	t (min)	^{40}Ar, 10^{-9} cm^3 STP	^{40}Ar/^{39}Ar	±1σ	^{38}Ar/^{39}Ar	±1σ	^{37}Ar/^{39}Ar	±1σ	^{36}Ar/^{39}Ar	±1σ	Ca/K	$\sum^{39}$Ar (%)	Age, Ma	±1σ
800	10	207.15	338.19	0.92	0.0366	0.0036	0.026	0.0163	0.0819	0.0015	0.092	4.5	1615.0	13.4
900	10	653.33	341.99	0.42	0.0295	0.00094	0.0082	0.0042	0.0554	0.00108	0.0296	14.3	1654.1	13.3
950	10	725.87	387.25	0.39	0.0282	0.00086	0.0197	0.0045	0.0564	0.00081	0.071	23.9	1797.7	13.9
980	10	851.55	484.19	0.43	0.0311	0.0014	0.0049	0.0037	0.06	0.00105	0.0178	33.0	2070.5	15.0
1000	10	766.97	518.62	0.46	0.0317	0.00081	0.0091	0.0025	0.0771	0.00068	0.0328	40.6	2146.4	15.3
1020	10	681.26	539.22	0.46	0.0277	0.00028	0.0144	0.0066	0.0743	0.00077	0.0519	47.1	2199.9	15.5
1040	10	1195.4	543.76	0.82	0.0326	0.00059	0.0032	0.0040	0.0814	0.0011	0.0114	58.4	2205.9	15.6
1050	10	2196.2	564.54	0.83	0.038	0.00073	0.0079	0.0045	0.1201	0.00129	0.0285	78.4	2228.6	15.7
1050	10	349.27	572.96	1.66	0.0318	0.0034	0.017	0.0124	0.0788	0.00334	0.0612	81.5	2277.8	16.3
1060	10	925.45	576.19	0.57	0.0336	0.00058	0.0006	0.0036	0.0729	0.00103	0.0023	89.8	2289.5	15.8
1070	10	762.07	582.61	0.78	0.0336	0.0014	0.0113	0.0045	0.0849	0.00159	0.0406	96.5	2296.2	15.9
1080	10	304.65	556.59	1.32	0.0337	0.003	0.0437	0.0111	0.0981	0.00172	0.1574	99.3	2225.1	15.9
1100	10	69.209	518.24	7.038	0.0509	0.0082	0.0523	0.0219	0.0935	0.00688	0.1883	100	2133.2	23.3
∀B300/09 phlogopite (1.19 mg), J = 0.004571 ± 0.000055; TFA = 2122 ± 15 Ma														
500	10	5.77	359.81	7.37	0.2394	0.0536	0.267	0.8766	0.5348	0.0922	0.961	0.9	1179.0	117.9
700	10	20.14	138.78	1.70	0.0177	0.0105	0.165	0.0487	0.0193	0.0081	0.592	9.1	857.3	17.0
850	10	38.93	231.02	1.71	0.0346	0.0045	0.095	0.0680	0.0449	0.0082	0.344	18.7	1246.3	16.2
975	10	120.08	477.96	1.58	0.0433	0.0072	0.057	0.0382	0.0549	0.0044	0.207	32.9	2047.3	15.7
1050	10	142.64	586.77	3.28	0.0413	0.0072	0.035	0.0311	0.0443	0.0023	0.125	46.7	2322.0	17.4
1130	6	558.17	593.08	1.002	0.0233	0.00129	0.021	0.0088	0.0265	0.00098	0.075	100	2348.2	16.0

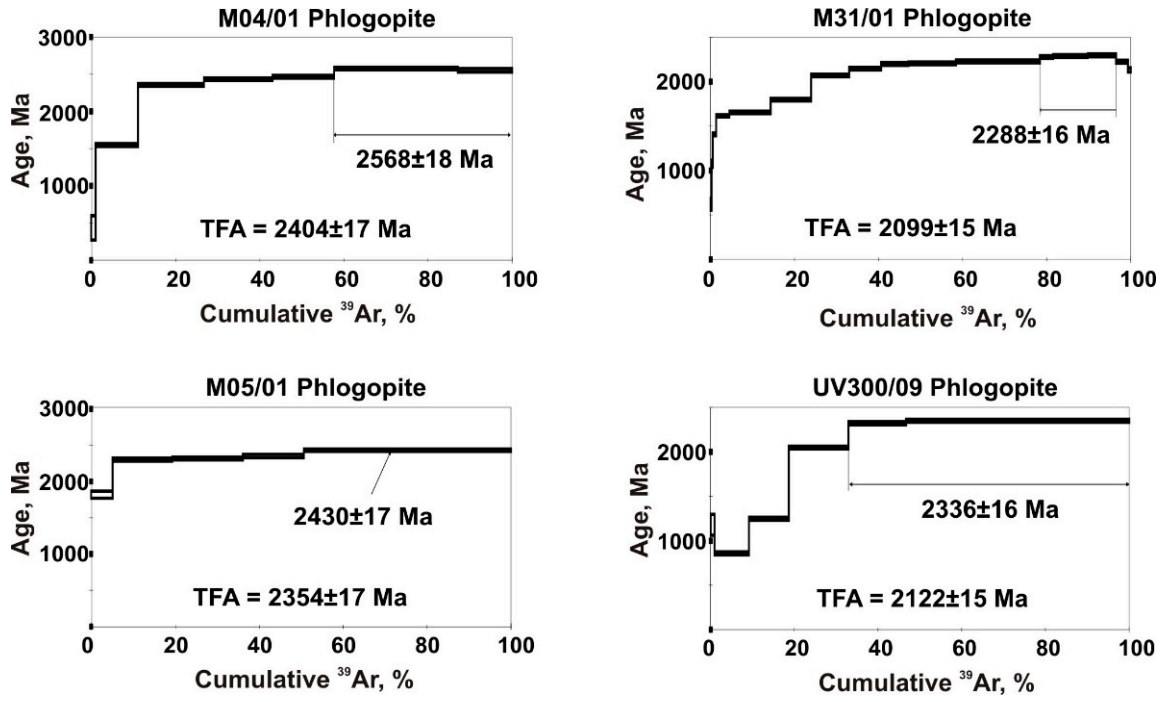

Figure 2. ^{40}Ar/^{39}Ar age spectra obtained for phlogopites from deep xenoliths of the Mir (Samples M4/01, M5/01, M31/01) and Udachnaya–Vostochnaya (Sample UV300/09) kimberlite pipes.

Table 2. Types of rocks and estimates of temperatures and pressures of the last equilibrium for phlogopite-containing xenoliths from kimberlite Mir (M4/01, M5/01, M31/01) and Udachnaya–Vostochnaya (UV300/09) pipes.

Sample	Rock	T, °C	P, GPa
M4/01	spinel-garnet olivine websterite	560 *	2.8 *
M5/01	garnet websterite	690 **	2.0 **
M31/01	garnet olivine websterite	890 **	4.3 **
УВ300/09	garnet-olivine clinopyroxenite	895 *	3.7 *

Note: PT-parameters are computed according to [50] (*), [51] (**).

3.2. Morphology, Composition, and Structural Features of Phlogopites Prior to and after Laboratory Experiments

Phlogopites from magnesial skarns of the Aldanian shield and Kuhi-Lal field (Tajikistan, SW Pamir) have a homogeneous chemical composition and contain no inclusions (Table 3, Figure 3). Phlogopite from the Aldanian shield skarns contains (% wt): FeO ~6, Na_2O~0.3, MnO~0.1, TiO_2~0.6, BaO~0.6, F—1.2−1.5, Cl~0.2. Phlogopite from skarns of the Kuhi-Lal field contains almost no FeO (<0.06% wt) and is characterised by the presence of the following admixtures (% wt): N_2O~1.3, TiO_2~0.7, BaO~0.1; the content of F and Cl therein is ~1.3 and ~0.05% wt, respectively (Table 3).

According to the results of SEM-observations, no changes in the morphology of phlogopites heat-treated at high pressures were detected, particularly, no signs of recrystallisation, solid-phase transformations, or melting were noticed (Figure 3). No significant differences in amounts of components in compositions of original and heat-treated phlogopites were identified that would indirectly indicate that a mineral had lost water while being heat-treated. No other significant differences in compositions of original and heated phlogopites were found (Table 3) as well.

The parameters of cells of phlogopites, heat-treated at high pressures, in general, alter slightly as compared to those of the original mica (except for specimens, heat-treated at 700 °C) (Table 4). This indicates that high-pressure heating led to no meaningful transformations in the structure of phlogopites (deformities and rotations of tetrahedral and octahedral polyhedrons, reduction of interlayer space [52–55]).

Table 3. Representative microprobe analyses (wt %) of phlogopites from magnesian skarns of the Aldan shield (**A**) and Kuhi-Lal field (Tajikistan, SW Pamir, **T**), original and heat-treated at 3 GPa pressure.

No. of Specimen	A 800 °C, 2 h	A 850 °C, 2 h	A 1000 °C, 2 h	A	A 700 °C, 72 h	A 800 °C, 72 h	A 900 °C, 72 h	A 1000 °C, 72 h
SiO_2	37.74	37.97	38.03	38.31	37.84	38.39	37.96	38.12
TiO_2	0.62	0.60	0.61	0.59	0.59	0.63	0.62	0.60
Cr_2O_3	bdl	bdl	bdl	bdl	bdl	bdl	bdl	bdl
Al_2O_3	16.71	16.62	17.14	16.48	16.63	16.80	16.72	16.50
FeO	6.10	6.01	6.07	5.96	6.10	6.30	6.05	6.22
MnO	0.06	0.07	0.07	0.05	0.06	0.06	0.07	0.07
MgO	22.50	22.37	22.76	22.88	22.80	23.12	22.89	22.62
CaO	0.03	0.06	bdl	bdl	bdl	bdl	bdl	bdl
BaO	0.59	0.63	0.47	0.62	0.72	0.55	0.66	0.68
Na_2O	0.28	0.33	0.29	0.34	0.31	0.36	0.33	0.33
K_2O	9.94	10.06	10.13	9.58	9.89	9.88	9.92	9.70
RbO	0.03	bdl	bdl	bdl	bdl	bdl	bdl	bdl

Table 3. *Cont.*

No. of Specimen	A 800 °C, 2 h	A 850 °C, 2 h	A 1000 °C, 2 h	A	A 700 °C, 72 h	A 800 °C, 72 h	A 900 °C, 72 h	A 1000 °C, 72 h
F	1.35	1.34	1.38	1.19	1.48	1.39	1.40	1.38
Cl	0.19	0.22	0.20	0.22	0.19	0.17	0.20	0.20
Total	95.53	95.67	96.52	95.83	96.06	97.07	96.28	95.91
Si	2.742	2.755	2.730	2.772	2.737	2.742	2.736	2.764
^{IV}Al	1.258	1.245	1.270	1.228	1.263	1.258	1.264	1.236
Ti	0.034	0.033	0.033	0.032	0.032	0.034	0.034	0.033
Fe^{2+}	0.371	0.365	0.364	0.361	0.369	0.376	0.365	0.377
^{VI}Al	0.173	0.178	0.181	0.177	0.155	0.157	0.157	0.174
Mn	0.004	0.004	0.004	0.003	0.004	0.004	0.005	0.004
Mg	2.436	2.420	2.435	2.467	2.458	2.461	2.459	2.444
Σoct	3.018	3.000	3.018	3.040	3.019	3.033	3.020	3.031
Ca	0.002	0.005	0.000	bdl	bdl	bdl	bdl	bdl
Ba	0.017	0.018	0.013	0.018	0.020	0.015	0.019	0.019
Na	0.040	0.047	0.041	0.048	0.043	0.050	0.047	0.046
K	0.921	0.931	0.928	0.884	0.913	0.901	0.912	0.897
Σ K	0.982	1.000	0.982	0.960	0.981	0.967	0.980	0.969
F	0.310	0.308	0.313	0.273	0.339	0.315	0.318	0.316
Cl	0.023	0.027	0.024	0.027	0.023	0.021	0.025	0.024
No. of Specimen	T	T**700 °C, 72 h**	T**800 °C, 72 h**	T**900 °C, 72 h**	T**1000 °C, 72 h**			
SiO_2	40.19	40.14	40.24	39.97	40.73			
TiO_2	0.72	0.74	0.56	0.64	0.79			
Cr_2O_3	0.05	0.04	0.04	<0.01	0.05			
Al_2O_3	15.98	15.47	16.68	16.31	15.36			
FeO	0.04	0.05	0.05	0.06	0.03			
MgO	26.58	27.12	27.00	27.00	26.98			
BaO	0.07	0.13	0.10	0.20	0.10			
Na_2O	1.08	0.88	1.24	1.08	0.81			
K_2O	8.83	9.32	8.79	9.01	9.34			
Rb_2O	<0.04	<0.04	0.06	<0.04	<0.04			
F	1.29	1.56	1.25	1.26	1.76			
Cl	0.04	0.05	0.04	0.08	0.07			
Total	94.35	94.92	95.53	95.10	95.32			
Si	2.854	2.838	2.815	2.813	2.877			
^{IV}Al	1.146	1.162	1.185	1.187	1.123			
Ti	0.038	0.039	0.029	0.034	0.042			
Fe^{2+}	0.002	0.003	0.003	0.003	0.002			
^{VI}Al	0.192	0.127	0.191	0.166	0.156			
Mg	2.813	2.858	2.816	2.832	2.840			

Table 3. *Cont.*

No. of Specimen	T	T700 °C, 72 h	T800 °C, 72 h	T900 °C, 72 h	T1000 °C, 72 h
Σoct	3.049	3.030	3.042	3.037	3.043
Ba	0.002	0.004	0.003	0.005	0.003
Na	0.149	0.120	0.169	0.148	0.111
K	0.800	0.841	0.784	0.809	0.841
Σ_K	0.951	0.970	0.958	0.963	0.957
F	0.290	0.348	0.276	0.281	0.394
Cl	0.005	0.006	0.005	0.009	0.008

Note: bdl = below the detection limit; **A**—phlogopite from skarns of the Aldan shield; Cr_2O_3 and CaO content on average <0.01% wt, Rb_2O content on average <0.04% wt; ^{IV}Al, ^{VI}Al—tetrahedral and octahedral Al. T—phlogopite from Tajikistan skarns; MnO content <0.01% wt, CaO content on average <0.01% wt; ^{IV}Al, ^{VI}Al—tetrahedral and octahedral Al.

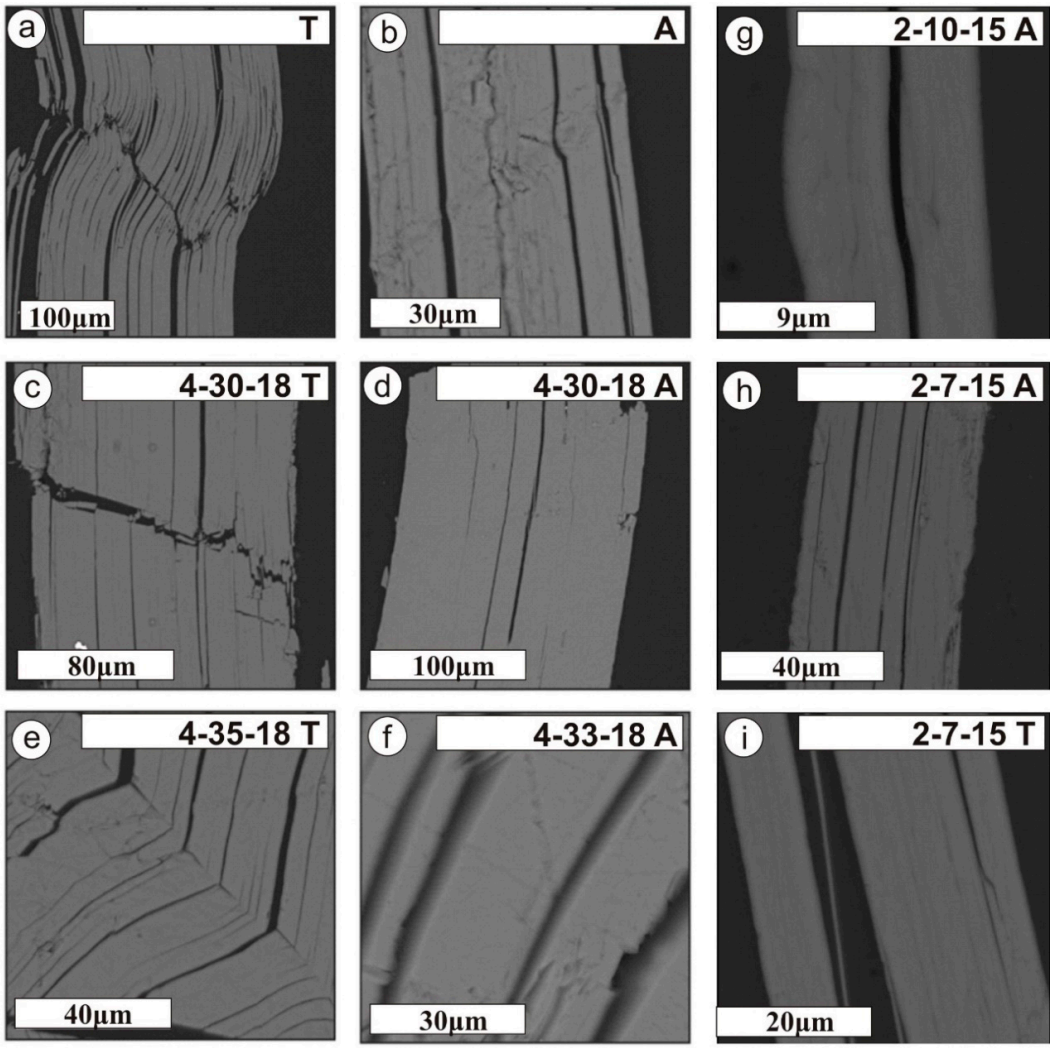

Figure 3. Morphology of original and heat-treated at high temperatures and pressures phlogopites (3 GPa) (BSE-photo, polished compounds). T—phlogopite from Tajikistan skarns, A—phlogopite from skarns of the Aldanian shield; (**a**,**b**)original specimens; (**c**–**i**)heat-treated specimens. Sp. 4-30-18—specimen, heat-treated at the temperature of 1000 °C during 72 h; sp. 4-35-18—specimen, heat-treated at the temperature of 800 °C during 72 h; sp. 4-33-18—specimen, heat-treated at the temperature of 900ºC during 72 h; sp. 2-10-15—specimen, heat-treated at the temperature of 850 °C during 2 h; sp. 2-7-15—specimen, heat-treated at the temperature of 1000 °C during 2 h.

Table 4. Parameters of the unit cell of the initial and heated at high temperatures and pressures (3 GPa) phlogopites.

N_o	**A (Initial)**	**A 700 °C, 72 h**	**A 800 °C, 72 h**	**A 900 °C, 72 h**	**A 1000 °C, 72 h**	**T(Initial)**	**T700 °C, 72 h**	**T800 °C, 72 h**	**T900 °C, 72 h**	**T1000 °C, 72 h**
a, Å	5.3301 ± 0.0003	5.3322 ± 0.0005	5.3422 ± 0.0003	5.3373 ± 0.0005	5.3199 ± 0.0004	5.3229 ± 0.0008	5.3836 ± 0.0024	5.3188 ± 0.0010	5.3366 ± 0.0019	5.3186 ± 0.0017
b, Å	9.2322 ± 0.0004	9.1994 ± 0.0025	9.2448 ± 0.0003	9.2203 ± 0.0014	9.2184 ± 0.0010	9.1876 ± 0.0047	9.2182 ± 0.0008	9.2114 ± 0.0015	9.2034 ± 0.0040	9.2112 ± 0.0057
c, Å	10.2424 ± 0.0004	10.2549 ± 0.0008	10.2481 ± 0.0003	10.2639 ± 0.0007	10.2499 ± 0.0005	10.2593 ± 0.0017	10.2442 ± 0.0006	10.2421 ± 0.0013	10.2488 ± 0.0009	10.2538 ± 0.0014
β, °	100.0944 ± 0.0065	100.4084 ± 0.0156	100.1893 ± 0.0050	100.3785 ± 0.0146	99.8768 ± 0.0079	100.6716 ± 0.0265	100.4040 ± 0.0197	100.3047 ± 0.0334	100.2990 ± 0.0375	100.3638 ± 0.0457
V, Å^3	496.2102 ± 0.0306	494.7522 ± 0.1319	498.1426 ± 0.0317	496.8366 ± 0.0885	495.2188 ± 0.0550	493.0516 ± 0.2382	500.0320 ± 0.2071	493.7001 ± 0.1113	495.2574 ± 0.3390	494.1426 ± 0.3101

Note: A—phlogopite from skarns of the Aldan shield; T—phlogopyte from the Kuhi-Lal ore field (Tajikistan, South Pamir).

To assess the degree of dihydroxylation in phlogopites from the first series of laboratory experiments (2 h long each), the Raman spectroscopy method was employed. A 3600−3780 cm^{-1} area of the Raman spectra of original phlogopites and all phlogopites, heat-treated at high pressures and temperatures, contains lines, conforming to vibrations in OH-groups. The intensities of these lines in the Raman spectra of original and heat-treated phlogopites are similar (Figure 4A,B). It can be inferred from these data that, at high-pressure 2 h long heating, dihydroxylation in phlogopites was minor.

To assess the degree of dihydroxylation in phlogopites from the second series of experiments (72 h), an infrared-spectroscopy method was used. IR-spectra of heat-treated specimens are similar to the spectra of original phlogopite specimens. IR-spectra of original micas within~3630−3780 cm^{-1} spectral range have two peaks of various intensity, that correspond to vibrations of hydroxyl ion, coordinated with di- and trivalent cations. IR-spectra of heat-treated phlogopites within this range have changes in the form and intensity of bands, that correspond to vibrations of $MgFe_2$+R_3+MgOH links. More intense transformations—dihydroxylation (perhaps, due to Fe^{2+} oxidation)—are seen in the phlogopite from skarns of the Aldanian shield (Figure 4D). Phlogopite from Kuhi-Lal field (Tajikistan), almost without iron, underwent smaller changes (Figure 4C).

The results of $^{40}Ar/^{39}Ar$ dating of phlogopite specimens prior to and after laboratory experiments are given in Table 5, in Figure 5. If standard plateaux with respective age values are seen in the spectra of original phlogopites, then as the intensity of influence increases, on one hand, measured values in the "Tadjik" phlogopite spectra raise, on the other hand, rejuvenation in the "Aldanian" phlogopite spectra takes place (Figure 5). Hence, it can be concluded that even in "close-to-real" laboratory conditions, there is an efficient mechanism of introducing radiogenic argon, released from the ancient phlogopite lattice, into the structure of younger phlogopite. It supports the assumption we have previously made that a mechanism exists for the effective exchange of radiogenic argon between phlogopite grains in the mantle conditions. On the other hand, due to a substantially higher concentration of radiogenic argon in the ancient phlogopite, the measured kinetics of its releasing can be utilised to estimate the parameters of argon diffusion in the mineral lattice.

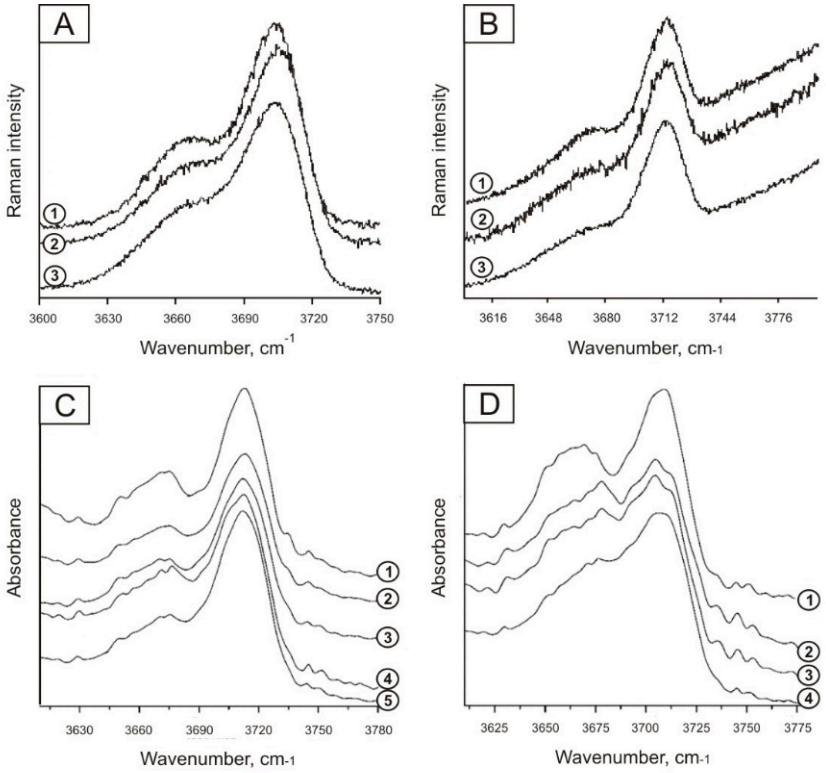

Figure 4. Raman spectra (R) and IR-spectra (**A**) Raman spectra of original and heat-treated at high temperatures and pressure of 3 GPa phlogopites in the area of stretching vibrations of OH-groups (phlogopite from the Aldanian shield rocks): 1—original specimen; 2—specimen, heat-treated at T = 850 °C, 2 h; 3—specimen, heat-treated at T = 1000 °C, 2 h. (**B**). Raman spectra of original and heat-treated at high temperatures and pressure 3 GPa phlogopites in the area of stretching vibrations of OH-groups (phlogopite from the Kuhi-Lal field rocks (Tajikistan)): 1—original specimen; 2—specimen, heat-treated at T = 850 °C, 2 h; 3—specimen, heat-treated at T = 1000 °C, 2 h. (**C**). Fragments of IR-spectra of original and heat-treated at high temperatures and pressure 3 GPa phlogopites in the area of stretching vibrations of OHgroups (phlogopite from the Kuhi-Lal field rocks (Tajikistan, SW Pamir)): 1—original specimen; 2—specimen, heat-treated at T = 700 °C, 72 h; 3—specimen, heat-treated at T = 800 °C, 72 h; 4—specimen, heat-treated at T = 900 °C, 72 h; 5—specimen, heat-treated at T = 1000 °C, 72 h. (**D**). Fragments of IR-spectra of original and heat-treated at high temperatures and pressure 3 GPa phlogopites in the area of stretching vibrations of OHgroups (phlogopite from magnesial skarns of the Aldanian shield): 1—original specimen; 2—specimen, heat-treated at T = 800 °C, 72 h; 3—specimen, heat-treated at T = 900 °C, 72 h; 4—specimen, heat-treated at T = 1000 °C, 72 h.

Figure 6 presents the Arrhenius diagram, obtained from the results of laboratory experiments. Resultant experimental points correspond well with the theoretical line for argon diffusion at 30 kbar pressure.

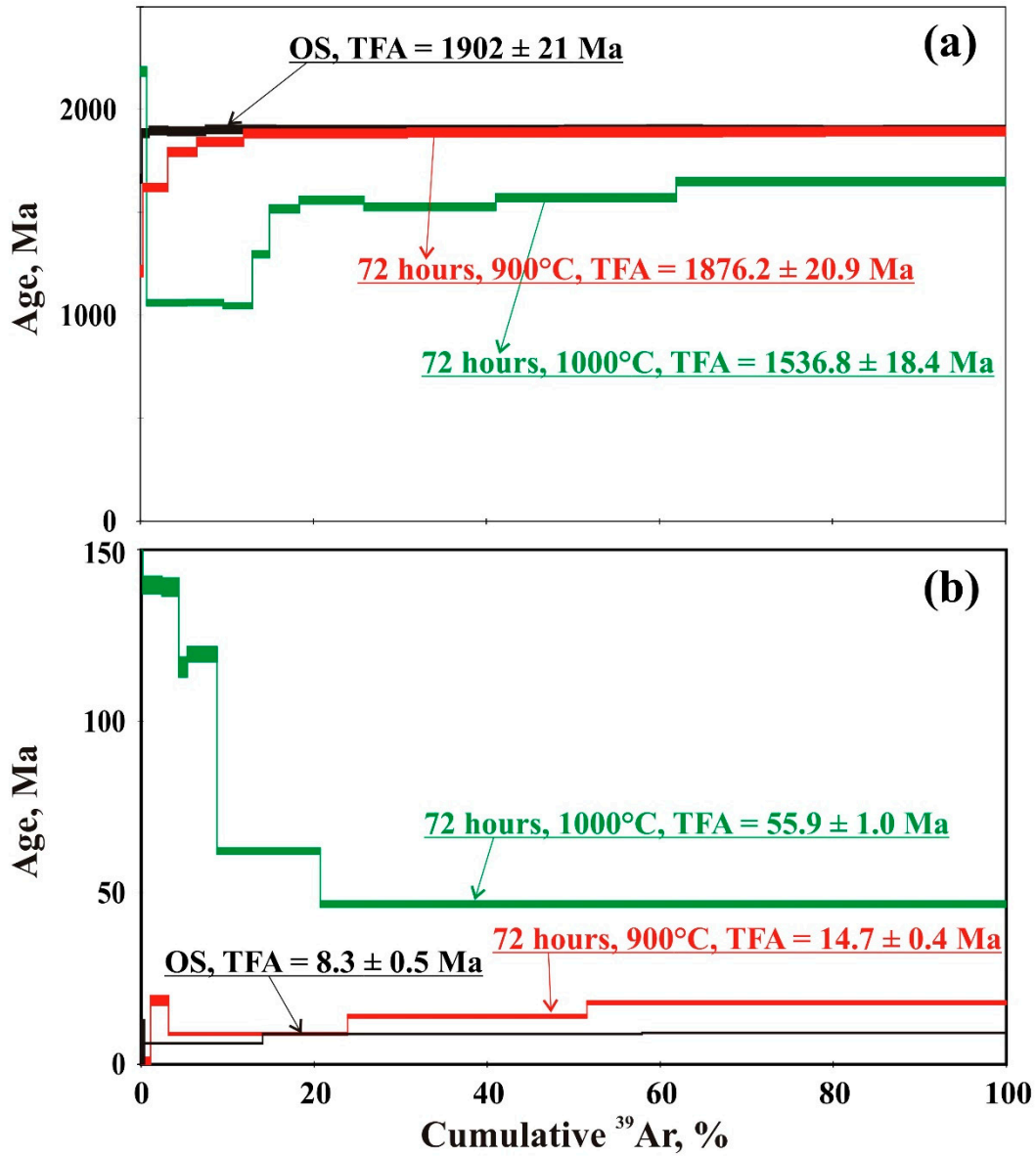

Figure 5. $^{40}Ar/^{39}Ar$ age spectra obtained by phlogopite (**a**) from the Aldanian shield rocks, (**b**) from the Kuhi-Lal field (Tajikistan) original and heat-treated at high temperatures and 3 GPa pressure. Parameters of the experiment and the values of integral age (TFA) are written in the figure. OS—original specimen.

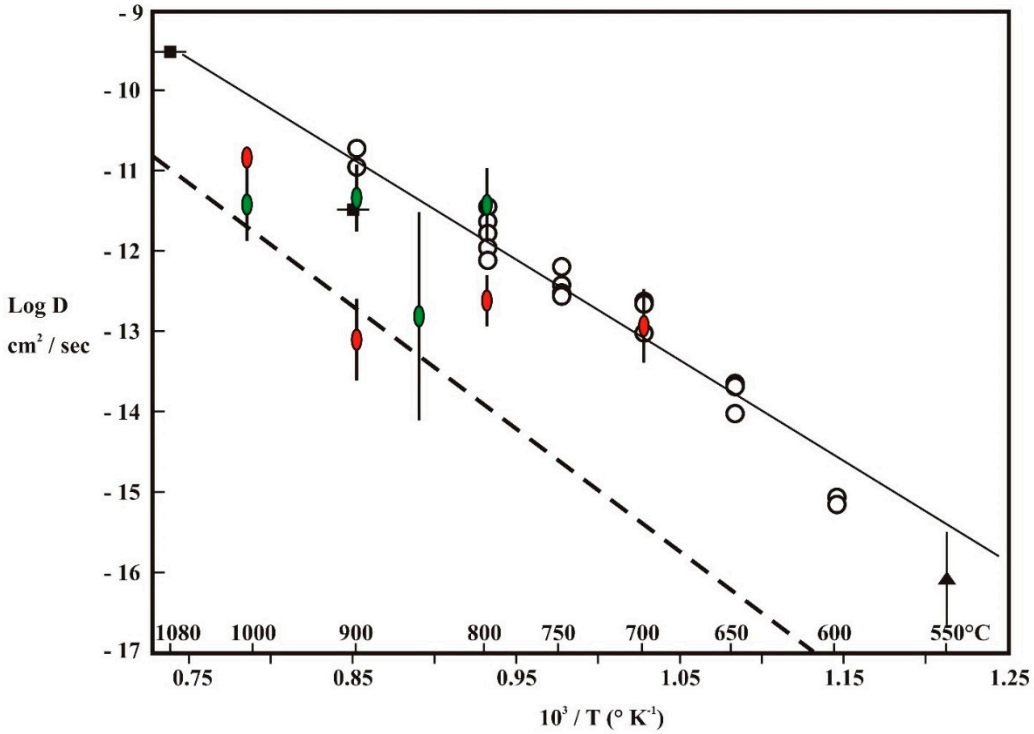

Figure 6. Arrhenius plot for radiogenic argon diffusion in phlogopite mica. Open circles and line are for data reported in [56] where all data are for 2 kbar water pressure except at 900 °C where they are for 1 kbar. Line has D_O = 0.75 cm^2/s and Ea = 242,672 J/mol. The two squares at 900 °C and 1080 °C are for runs at 15 kbar water pressure. The solid triangle at 550 °C was for a 1 bar water pressure run.

Our experimental data: Green—laboratory experiment duration 2 h and pressure 3 GPa; Red—laboratory experiment: duration 72 h and pressure 3 GPa; the dotted line is designed for a pressure of 30 kbar taking into account the known kinetic parameters of the phlogopite [23] and is characterized by D_O = 0.75 cm^2/sec and E_a = 284,672 J/mol for 3 GPa (activation volume—14 cm^3/mol [23]).

4. Numerical Simulation

Numerical simulation of the K/Ar isotopic system behaviour in phlogopite was based on argon mobility, described by the law of "volume thermally activated diffusion". Kinetic parameters of argon mobility in phlogopite: activation energy—242672 J/mol, pre-exponential factor—7.5e^{-5} m^2/sec, diffusion domain size—150 µm, activation volume—14 cm^3/mol [22,56–59].

When modelling the K/Ar isotopic system behaviour, a change in the content of radiogenic argon in the mineral lattice is considered, defined by the superposition of two factors: accumulation of ^{40}Ar due to radioactive ^{40}K decay and argon diffusion as per the second Fick's law. The general form of the obtained diffusion equation is as follows:

$$\frac{dC_{Ar}\left(\vec{r},t\right)}{dt} = \nabla \cdot \left(D(r,P,T(t))\nabla C_{Ar}\left(\vec{r},t\right)\right) - \frac{dC_K(t)}{dt} \quad (1)$$

where $C_{Ar}\left(\vec{r},t\right)$—distribution of radiogenic argon isotope distribution, D—diffusion coefficient, $C_K(t)$—distribution of potassium concentration in mineral grains, defined by the law of radioactive decay: $C_K(t) = C_{K0}e^{-\lambda t}$.

Diffusion coefficient depends on both temperature, and pressure according to the Arrhenius law: $D(P,T) = D_0 e^{-\frac{E_a+PV_a}{RT}}$,

where D_0—pre-exponential factor, E_a—activation energy, P—ambient pressure, V_a—activation volume, R—universal gas constant, T—temperature.

Since phlogopite has a cylindrical symmetry, it seems logical to convert the equation to cylindrical coordinate system. At the grain–inter-grain space interface, there is a jump in the diffusion coefficient from D in the grain to some effective value of diffusion coefficient D_{eff} in the inter-grain space. As $D_{eff} >> D$, argon rapidly propagates throughout the inter-grain space. Equation (1) will take the form:

$$\frac{dC_{Ar}(r,t)}{dt} = D(r,P,T(t))\left(\frac{d^2C_{Ar}(r,t)}{dr^2} + \frac{1}{r}\frac{dC_{Ar}(r,t)}{dr}\right) + \frac{dD(r,P,T(t))}{dr}\frac{dC_{Ar}(r,t)}{dr} + \lambda C_{K0}e^{-\lambda t} \quad (2)$$

When diffusion coefficient changes stepwise, term $\frac{dD(r,P,T(t))}{dr}\frac{dC_{Ar}(r,t)}{dr}$ is a boundary condition of the 3rd type for the grain–inter-grain space interface, i.e., this condition will be taken into account automatically when solving differential Equation (2), and it need not be further introduced.

To construct a numerical algorithm for solving Equation (2), Euler's method was employed. The algorithm was implemented using a package of MatLab mathematical programs (MATLAB 7).

We used Equation (2), with specifying respective initial and boundary conditions, both in numerical simulation of the evolution of the K/Ar isotopic system of phlogopite in conditions of a high-pressure laboratory experiment, and in numerical calculations of the model, describing the evolution of the K/Ar isotopic system of phlogopite from its origination at depth to transporting to the earth's surface by the kimberlite melt.

Work [60] presents the MacArgon software programme for Apple Macintosh to model the effect of P-T-t history on the diffusion of argon in minerals.

5. Discussion

The results of numerical simulation of the behaviour observed in the K/Ar isotopic system of phlogopite in various conditions of the laboratory experiment are given in Figure 7. Comparing them with the experimental data of $^{40}Ar/^{39}Ar$ dating of phlogopites prior to and after high-pressure laboratory heating (Table 5, Figure 7b,c) provides a good fit within the limits of error for all experiments, except for one—3 GPa, 1000 °C, 72 h. In the last experiment, 340 Ma rejuvenation of the K/Ar isotopic system of phlogopite was achieved, which is markedly higher than the numeric estimate of the loss. Conceivably, this is because of a large degree of dihydroxylation in phlogopite in the course of this laboratory experiment, which is also proved by the IR-spectroscopy data (Figure 4D). Reconciliation of the numerical simulation data with the laboratory experiment data enables the conclusion to the drawn that the mechanism of the mobility of radiogenic argon in phlogopite lattice—volume diffusion, incorporated into the numerical simulation, is justified.

It can be seen that even considering the addition to the energy of argon diffusion activation, associated with pressure at depth, several hours of heating suffice for a considerable loss of radiogenic argon at temperatures exceeding 850 °C. This is in conflict with the fact that the K/Ar isotopic system of phlogopite from deep-seated xenoliths M-31/01 (formation temperature ~890 °C, Table 2), UV-300/09 (formation temperature ~895 °C, Table 2), despite their long (at least 2 billion years) exposure in the mantle conditions, retained the memory of their formation age. Apparently, this phenomenon is explained by constrained sinks for radiogenic argon from phlogopite in the mantle conditions.

In view of the above-said, when describing the evolution of the K/Ar isotopic system of phlogopite, from its origination at depth in the mantle conditions to transporting it to the Earth's surface in the kimberlite melt, applying numerical simulation, we considered three stages and assumed boundary conditions, according to the phlogopite position:

Stage 1. The grain is a part of a deep-seated block of rocks. The value of temperature and pressure is assumed to be in line with estimates, obtained for each examined xenolith (Table 2). It is supposed that the grain exchanges argon with other grains through the inter-grain space, which leads to the accumulation of some amount of radiogenic argon

in the inter-grain space. Hence, suppose that, around the grain, some area in the space exists, where the total flow of argon from adjacent grains becomes equal to the counter flow from the grain itself, i.e., a boundary is formed, at which the total flow of argon is zero. Then, based on the first Fick's law: $q = -D\vec{\nabla}C$ (the flow rate is directly proportional to the diffusion coefficient and negative gradient)—we obtain that the concentration gradient of radiogenic argon at the interface of computation area is zero.

Stage 2. Xenolith with phlogopite is in the kimberlite melt (due to the small sizes of xenolith with respect to the original rock). We have a zero boundary condition to retain argon at the interface of phlogopite grain, computation area therewith reduces the diffusion domain sizes. The kimberlite melt temperature is assumed to be 1000 °C [26]. Pressure changes linearly, from the value obtained by mineral geobarometer for each examined xenolith, to 0.0001 GPa in the Earth's surface.

Stage 3. After the kimberlite body had been formed on the surface, the phlogopite temperature is lower than the closure temperature of its K/Ar isotopic system. Radiogenic ^{40}Ar is accumulated due to ^{40}K radioactive decay.

Comparison between numerical simulation results and results of ^{40}Ar/^{39}Ar dating for phlogopites from deep-seated xenoliths

Phlogopite loses ^{40}Ar in the considered model only at the 2nd stage, namely, during the xenolith ascent in the kimberlite melt to the surface. At the 1st and 3rd stages, the mere accumulation of radiogenic ^{40}Ar takes place according to the law of radioactive decay.

A typical shape in the ^{40}Ar/^{39}Ar age spectrum in the form of an "up staircase" is an indicator of the partial loss of radiogenic ^{40}Ar for specimens of phlogopites from deep-seated xenoliths (Table 1, Figure 2). In terms of quantity, the degree of ^{40}Ar loss is estimated based on the difference in Ma between the age value of the highest temperature step in the age spectrum (the closest to the initial age) and integral age. For instance, for specimen M05/01 this difference is 75.9 Ma, for UV300/09—215 Ma. It can be noted that this value correlates well with PT-estimates for the analysed xenoliths (Table 2). The greater the depth, from which xenolith with phlogopite came, the greater the loss of radiogenic argon.

Figure 8 presents a model dependence of the calculated degree of radiogenic ^{40}Ar loss by phlogopite on the ascent rate of xenolith in the kimberlite melt. For each xenolith, ascent had started from the depth of its formation, depending on the estimate of pressure in a state of the last equilibrium (Table 2). An option of rising at a constant rate was considered. The slower the rate, the longer the time for rock heating at the melt temperature (~1000 °C) and, respectively, the greater the loss of radiogenic ^{40}Ar. An optimum ascent rate (Figure 8) was estimated from the intersection of the model value and the value, calculated according to the age ^{40}Ar/^{39}Ar spectrum of phlogopite, of the loss for each specimen. It can be seen that the obtained estimates of the kimberlite melt ascent rate (Figure 9) agree with one another for the two deep-seated xenoliths of the Mir pipe, and xenolith of the Udachnaya–Vostochnaya pipe. For xenolith M-05/01 of the Mir pipe from the depth of 66 km, a minimum loss of radiogenic ^{40}Ar was observed. This is quite likely to be the reason for a greater error in computing the ascent rate. On the other hand, a relatively inflated estimate for a xenolith from the shallowest depth can be associated with an increase in the melt ascent rate in the upper part of the continental crust, when overburden pressure falls. The weighted average of the rate of the kimberlite melt ascent for all the examined xenoliths is 16 ± 3 km/h.

Table 5. Results of $^{40}Ar/^{39}Ar$ Dating of phlogopite samples from magnesian skarns of the Aldan shield (**A**) and the Kuhi-Lal Deposit (Tajikistan, South Pamir, **T**) before and after laboratory experiments.

T °C	t m	^{40}Ar, 10^{-9} cm^3 STP	$^{40}Ar/^{39}Ar$	±1σ	$^{38}Ar/^{39}Ar$	±1σ	$^{37}Ar/^{39}Ar$	±1σ	$^{36}Ar/^{39}Ar$	±1σ	Ca/K	$\sum^{39}Ar$ (%)	Age, Ma	±1σ
Original phlogopite from magnesial skarns of the Aldanian shield, crystal edge, specimen A phlogopite (10.26 mg)														
J = 0.003832 ± 0.000038; TFA = 1902 ± 21 Ma														
500	10	177.2	302.9	0.585	0.089	0.00199	—	—	0.279	0.0019	—	0.2	1665.3	19.7
600	10	717.6	288.4	0.290	0.030	0.00077	—	—	0.068	0.0010	—	1.0	1887.4	21.0
700	10	1774.5	279.0	0.127	0.023	0.00021	—	—	0.026	0.0004	—	3.2	1900.2	21.0
800	10	3598.8	276.0	0.066	0.020	0.00015	—	—	0.019	0.0002	—	7.5	1896.4	21.0
850	10	6761.3	280.6	0.067	0.021	0.00008	—	—	0.028	0.0002	—	15.6	1905.1	21.0
875	10	10748.5	276.0	0.058	0.019	0.00008	—	—	0.014	0.0002	—	28.7	1902.3	21.0
900	10	11469.8	273.4	0.047	0.017	0.00007	—	—	0.007	0.0001	—	42.8	1900.8	21.0
925	10	5093.1	273.5	0.061	0.017	0.00007	—	—	0.006	0.0002	—	49.0	1902.7	21.0
950	10	7743.3	273.9	0.058	0.017	0.00006	—	—	0.006	0.0001	—	58.5	1904.5	21.0
975	10	5243.9	274.9	0.081	0.017	0.00009	—	—	0.008	0.0003	—	64.9	1905.9	21.0
1000	10	4304.6	275.8	0.080	0.018	0.00013	—	—	0.013	0.0002	—	70.2	1903.9	21.0
1025	10	4698.4	277.9	0.088	0.019	0.00010	—	—	0.020	0.0003	—	75.9	1903.9	21.0
1050	10	2474.2	280.5	0.074	0.022	0.00023	—	—	0.029	0.0002	—	78.8	1902.7	21.0
1090	10	5907.2	278.8	0.073	0.021	0.00008	—	—	0.026	0.0002	—	85.9	1899.6	21.0
1130	10	11577.2	276.5	0.054	0.019	0.00012	—	—	0.016	0.0002	—	100.0	1902.7	21.0
Original phlogopite from Kuhi-Lal field (Tajikistan, SW Pamir) specimen T phlogopite (6.58 mg)														
J = 0.00974 ± 0.000245; TFA = 8.3 ± 0.5 Ma														
800	10	31.7	5.1	0.004	0.016	0.0003	0.0344	0.0063	0.017	0.0005	0.124	1.9	2.2	2.6
900	10	132.9	3.3	0.001	0.016	0.0001	0.0004	0.0008	0.009	0.0002	0.001	14.5	8.6	1.0
1000	10	7.5	1.8	0.003	0.014	0.0005	0.0144	0.0057	0.005	0.0007	0.052	15.9	6.8	3.5
1050	10	182.8	1.3	0.001	0.015	0.00002	0.00001	0.000002	0.003	0.0002	0.00003	60.9	8.0	0.8
1075	10	69.5	0.9	0.001	0.015	0.00005	0.00001	0.00001	0.002	0.0002	0.00004	83.6	8.2	1.0
1130	10	59.5	1.1	0.001	0.015	0.00003	0.0006	0.0008	0.002	0.0002	0.002	100.0	9.7	1.1
Original phlogopite from magnesial skarns of the Aldanian shield, crystal edge, specimen A phlogopite (0.16 mg)														
J = 0.004134 ± 0.000045; TFA = 1876 ± 13 Ma														
1130	10	3159.4	452.5	0.164	0.023	0.0004	0.001	0.005	0.034	0.0003	0.005	100.0	1876.0	12.7
Original phlogopite from magnesial skarns of the Aldanian shield, crystal centre, specimen A phlogopite (0.32 mg)														
J = 0.004125 ± 0.000045; TFA = 1875 ± 13 Ma														
1130	10	5375.3	448.0	0.059	0.019	0.0002	0.008	0.002	0.017	0.0001	0.027	100.0	1874.6	12.7
Phlogopite from magnesial skarns of the Aldanian shield after laboratory experiment 2 h 3 GPa 800 °C, specimen 2-34-15 A phlogopite (0.13 mg)														
J = 0.004421 ± 0.000051; TFA = 1872 ± 13 Ma														
1130	10	2483.4	421.5	0.205	0.022	0.0003	1.050	0.440	0.031	0.0003	3.778	100.0	1872.4	13.5
Phlogopite from magnesial skarns of the Aldanian shield after laboratory experiment 2 h 3 GPa 900 °C, specimen 2-35-15 A phlogopite (0.18 mg)														
J = 0.004417 ± 0.000051; TFA = 1869 ± 13 Ma														
1130	10	2838.5	425.5	0.228	0.026	0.0001	1.481	0.273	0.047	0.0005	5.331	100.0	1869.4	13.5
Phlogopite from magnesial skarns of the Aldanian shield after laboratory experiment 2 h 3 GPa 850 °C, specimen 2-10-15 A phlogopite (4.46 mg)														
J = 0.004168 ± 0.000046; TFA = 1896 ± 13 Ma														
1130	10	69801.7	469.4	0.068	0.031	0.0001	0.944	0.140	0.078	0.0001	3.40	100.0	1896.0	13.0

Table 5. *Cont.*

Phlogopite from Kuhi-Lal field (Tajikistan, SW Pamir) after laboratory experiment 2 h 3 GPa 850 °C, specimen 2-10-15 T phlogopite (5.8 mg)														
J = 0.004149 ± 0.000045; TFA = 10.0 ± 0.2 Ma														
500	10	153.3	329.6	1.321	0.225	0.0033	0.013	0.045	1.085	0.0059	0.05	0.2	67.1	8.6
800	10	484.5	43.4	0.010	0.042	0.0001	0.017	0.003	0.141	0.0002	0.06	5.7	13.6	0.5
900	10	588.3	12.9	0.002	0.023	0.00005	0.305	0.085	0.039	0.0001	1.10	27.8	10.4	0.3
975	10	399.8	10.1	0.002	0.021	0.0000	0.547	0.151	0.030	0.0001	1.97	47.0	9.3	0.2
1050	10	418.5	8.5	0.002	0.020	0.0001	0.359	0.112	0.024	0.0001	1.29	70.8	9.9	0.2
1130	10	404.9	6.7	0.001	0.019	0.00002	0.0001	0.0006	0.019	0.0001	0.0003	100.0	9.4	0.2
Phlogopite from magnesial skarns of the Aldanian shield after laboratory experiment 2 h 3 GPa 1000 °C, specimen 2-7-15 A phlogopite (2.53 mg)														
J = 0.004158 ± 0.000045; TFA = 1872 ± 13 Ma														
1130	10	32022.3	449.6	0.078	0.023	0.0001	0.990	0.138	0.038	0.0001	3.56	100.0	1871.7	12.6
Phlogopite from Kuhi-Lal field (Tajikistan, SW Pamir) after laboratory experiment 2 h 3 GPa 1000 °C, specimen 2-7-15 T phlogopite (1.98 mg)														
J = 0.004141 ± 0.000045; TFA = 10.6 ± 0.2 Ma														
500	10	129.7	522.8	6.012	0.391	0.0091	24.977	10.297	1.760	0.0219	89.92	0.4	20.5	18.2
700	10	399.5	271.9	0.468	0.193	0.0011	7.404	1.659	0.914	0.0020	26.66	2.8	12.8	2.5
1000	10	1334.8	34.9	0.003	0.037	0.00003	0.001	0.0004	0.113	0.0001	0.004	66.0	11.7	0.2
1130	10	367.2	17.9	0.004	0.026	0.0001	0.237	0.128	0.057	0.0002	0.85	100.0	8.5	0.4
Phlogopite from magnesial skarns of the Aldanian shield after laboratory experiment 72 h 3 GPa 700 °C, specimen 4-36-18 A (5.28 mg)														
J = 0.006802 ± 0.000120; TFA = 1874 ± 21 Ma														
500	10	159.6	532.0	2.517	0.303	0.00491	3.007	0.648	1.1783	0.0073	10.824	0.2	1463.4	19.8
600	10	461.7	324.0	0.200	0.066	0.00095	0.704	0.085	0.2563	0.0006	2.536	1.4	1784.3	20.0
700	10	866.3	293.9	0.256	0.044	0.00045	0.128	0.101	0.1119	0.0009	0.460	3.9	1840.8	20.4
800	10	1587.0	281.0	0.086	0.028	0.00019	0.279	0.045	0.0500	0.0003	1.003	8.6	1864.5	20.5
900	10	8037.0	275.9	0.064	0.021	0.00010	0.013	0.010	0.0223	0.0002	0.045	32.8	1877.8	20.6
950	10	6254.9	272.3	0.051	0.018	0.00009	0.028	0.013	0.0113	0.0001	0.100	51.8	1876.6	20.6
Phlogopite from magnesial skarns of the Aldanian shield after laboratory experiment 72 h 3 GPa 800 °C, specimen 4-35-18 A (6.95 mg)														
J = 0.006864 ± 0.000123; TFA = 1857 ± 21 Ma														
500	10	273.8	538.3	2.037	0.263	0.00338	3.883	0.708	1.2570	0.0060	13.978	0.4	1377.2	18.7
600	10	618.7	306.2	0.290	0.071	0.00074	0.351	0.127	0.2735	0.0010	1.263	2.0	1686.5	19.7
700	10	966.0	298.3	0.146	0.047	0.00059	0.858	0.131	0.1724	0.0005	3.090	4.6	1790.4	20.4
800	10	1568.1	285.6	0.087	0.033	0.00020	0.001	0.000	0.0948	0.0003	0.005	9.0	1837.0	20.7
900	10	5805.9	278.4	0.053	0.026	0.00006	0.092	0.009	0.0548	0.0001	0.331	25.7	1857.3	20.8
950	10	5159.0	271.5	0.075	0.021	0.00009	0.065	0.020	0.0263	0.0002	0.232	41.0	1864.3	20.8
975	10	6338.4	270.6	0.038	0.019	0.00005	0.0003	0.0001	0.0209	0.0001	0.001	59.8	1867.3	20.8
1000	10	1107.4	269.9	0.131	0.023	0.00036	0.419	0.065	0.0245	0.0005	1.508	63.1	1859.4	20.8
1050	10	4853.9	271.1	0.057	0.020	0.00009	0.010	0.014	0.0227	0.0002	0.035	77.4	1867.0	20.8
1075	10	2012.1	271.0	0.073	0.019	0.00024	0.0410	0.0650	0.0242	0.0002	0.1475	83.4	1864.8	20.8
1130	10	5602.6	270.0	0.068	0.019	0.00007	0.0471	0.0164	0.0192	0.0002	0.170	100.0	1866.7	20.8

Table 5. *Cont.*

Phlogopite from magnesial skarns of the Aldanian shield after laboratory experiment 72 h 3 GPa 900 °C, specimen 4-33-18 A (4.02 mg)														
J = 0.006876 ± 0.000123; TFA = 1876±21 Ma														
500	10	84.2	430.0	1.796	0.234	0.00646	1.684	1.417	0.9816	0.0120	6.061	0.3	1216.1	26.6
600	10	553.4	283.2	0.229	0.068	0.00074	0.267	0.105	0.2406	0.0009	0.962	3.2	1622.8	19.2
700	10	665.9	293.0	0.210	0.047	0.00101	1.083	0.098	0.1525	0.0014	3.899	6.5	1795.1	20.4
800	10	1043.2	285.4	0.184	0.033	0.00045	0.229	0.085	0.0899	0.0008	0.826	11.9	1844.5	20.7
900	10	3589.8	280.1	0.064	0.025	0.00017	0.084	0.019	0.0414	0.0002	0.303	30.8	1884.3	20.9
950	10	3285.9	277.0	0.065	0.021	0.00020	0.037	0.030	0.0271	0.0001	0.134	48.4	1889.3	20.9
1000	10	3560.2	278.2	0.043	0.021	0.00011	0.029	0.022	0.0282	0.0002	0.103	67.2	1892.8	21.0
1050	10	2251.4	279.3	0.062	0.020	0.00016	0.004	0.034	0.0333	0.0003	0.014	79.1	1891.4	21.0
1130	10	3925.3	277.9	0.095	0.020	0.00007	0.043	0.016	0.0253	0.0001	0.156	100.0	1895.2	21.0
Phlogopite from magnesial skarns of the Aldanian shield after laboratory experiment 72 h 3 GPa 1000 °C, specimen 4-30-18 A (10.07 mg)														
J = 0.006855 ± 0.000122; TFA = 1537 ± 18 Ma														
500	10	506.1	621.0	0.812	0.207	0.00245	1.378	0.370	0.9393	0.0017	4.961	0.7	2183.5	22.6
600	10	762.5	144.8	0.066	0.037	0.00033	0.320	0.053	0.0957	0.0004	1.151	5.3	1059.3	14.3
700	10	703.8	145.9	0.076	0.036	0.00045	0.017	0.075	0.0983	0.0005	0.063	9.6	1061.5	14.3
800	10	540.3	142.2	0.066	0.035	0.00060	0.135	0.060	0.0939	0.0004	0.485	12.9	1044.9	14.1
850	10	423.0	185.6	0.142	0.036	0.00083	0.600	0.097	0.1093	0.0008	2.159	14.9	1295.8	16.5
900	10	913.8	232.4	0.109	0.044	0.00052	0.001	0.001	0.1363	0.0005	0.002	18.4	1516.0	18.3
950	10	1973.5	232.5	0.054	0.037	0.00019	0.097	0.035	0.1089	0.0002	0.350	25.8	1559.3	18.6
1000	10	3700.5	213.6	0.052	0.028	0.00012	0.031	0.019	0.0665	0.0002	0.110	41.1	1525.6	18.3
1050	10	5167.6	217.5	0.053	0.026	0.00007	0.027	0.008	0.0505	0.0002	0.097	61.9	1570.9	18.7
1130	10	9887.9	228.3	0.082	0.022	0.00003	0.0001	0.0001	0.0351	0.0001	0.0002	100.0	1648.8	19.2
Phlogopite from Kuhi-Lal field (Tajikistan, SW Pamir) after laboratory experiment 72 h 3 GPa 700 °C, specimen 4-36-18 T(6.35 mg)														
J = 0.006785 ± 0.000120; TFA = 9.4±0.2 Ma														
950	10	677.0	8.7	0.002	0.020	0.00002	0.058	0.012	0.0269	0.00003	0.207	58.5	9.5	0.2
1025	10	162.3	4.2	0.002	0.017	0.00004	0.0005	0.000	0.0119	0.0001	0.002	87.4	9.0	0.3
1130	10	109.6	6.5	0.003	0.019	0.00007	0.196	0.019	0.0194	0.0001	0.707	100.0	9.9	0.4
Phlogopite from Kuhi-Lal field (Tajikistan, SW Pamir) after laboratory experiment 72 h 3 GPa 800 °C, specimen 4-35-18 T(15.53 mg)														
J = 0.006832 ± 0.000121; TFA = 7.3 ± 0.2 Ma														
900	10	1284.1	36.2	0.007	0.038	0.00006	0.013	0.004	0.1217	0.0001	0.045	13.4	2.5	0.2
1000	10	2913.8	37.3	0.010	0.039	0.00002	0.014	0.005	0.1246	0.0001	0.050	42.8	6.1	0.2
1130	10	1312.3	8.6	0.002	0.021	0.00001	0.017	0.002	0.0267	0.00001	0.062	100.0	9.1	0.2
Phlogopite from Kuhi-Lal field (Tajikistan, SW Pamir) after laboratory experiment 72 h 3 GPa 900 °C, specimen 4-33-18 T(12.11 mg)														
J = 0.006881 ± 0.000123; TFA = 14.7 ± 0.4 Ma														
700	10	1294.5	499.2	0.265	0.343	0.00086	0.702	0.128	1.6894	0.0010	2.527	1.1	0.1	1.9
800	10	1050.6	207.9	0.085	0.151	0.00042	0.305	0.078	0.6984	0.0005	1.098	3.2	18.5	1.4
900	10	1688.7	33.8	0.004	0.036	0.00004	0.005	0.005	0.1119	0.0001	0.017	23.8	8.8	0.3
1000	10	2688.0	40.2	0.006	0.040	0.00003	0.014	0.003	0.1323	0.0001	0.049	51.5	13.9	0.5
1130	10	1896.5	16.2	0.004	0.025	0.00002	0.024	0.002	0.0498	0.0001	0.087	100.0	17.8	0.5

Table 5. *Cont.*

Phlogopite from Kuhi-Lal field (Tajikistan, SW Pamir) after laboratory experiment: 72 h 3 GPa 1000 °C, specimen 4-30-18 T(20.3 mg)														
J = 0.006844 ± 0.000122; TFA = 55.9 ± 1.0 Ma														
500	10	122.9	150.7	0.271	0.106	0.00203	0.024	0.375	0.4568	0.0019	0.085	0.2	184.5	6.5
600	10	472.0	64.4	0.019	0.050	0.00007	0.137	0.034	0.1782	0.0003	0.493	2.5	139.7	2.6
700	10	422.7	67.0	0.025	0.053	0.00013	0.079	0.039	0.1871	0.0004	0.283	4.4	139.1	2.7
800	10	223.8	69.7	0.045	0.056	0.00079	0.059	0.112	0.2030	0.0006	0.211	5.4	115.8	2.9
900	10	771.8	68.1	0.020	0.053	0.00017	0.032	0.019	0.1966	0.0002	0.116	8.8	119.5	2.2
1000	10	1225.2	31.3	0.005	0.032	0.00003	0.046	0.006	0.0888	0.0001	0.164	20.7	61.8	1.1
1130	10	5612.7	21.6	0.004	0.027	0.00001	0.023	0.001	0.0601	0.0001	0.083	100.0	46.5	0.9

"—"—not determined.

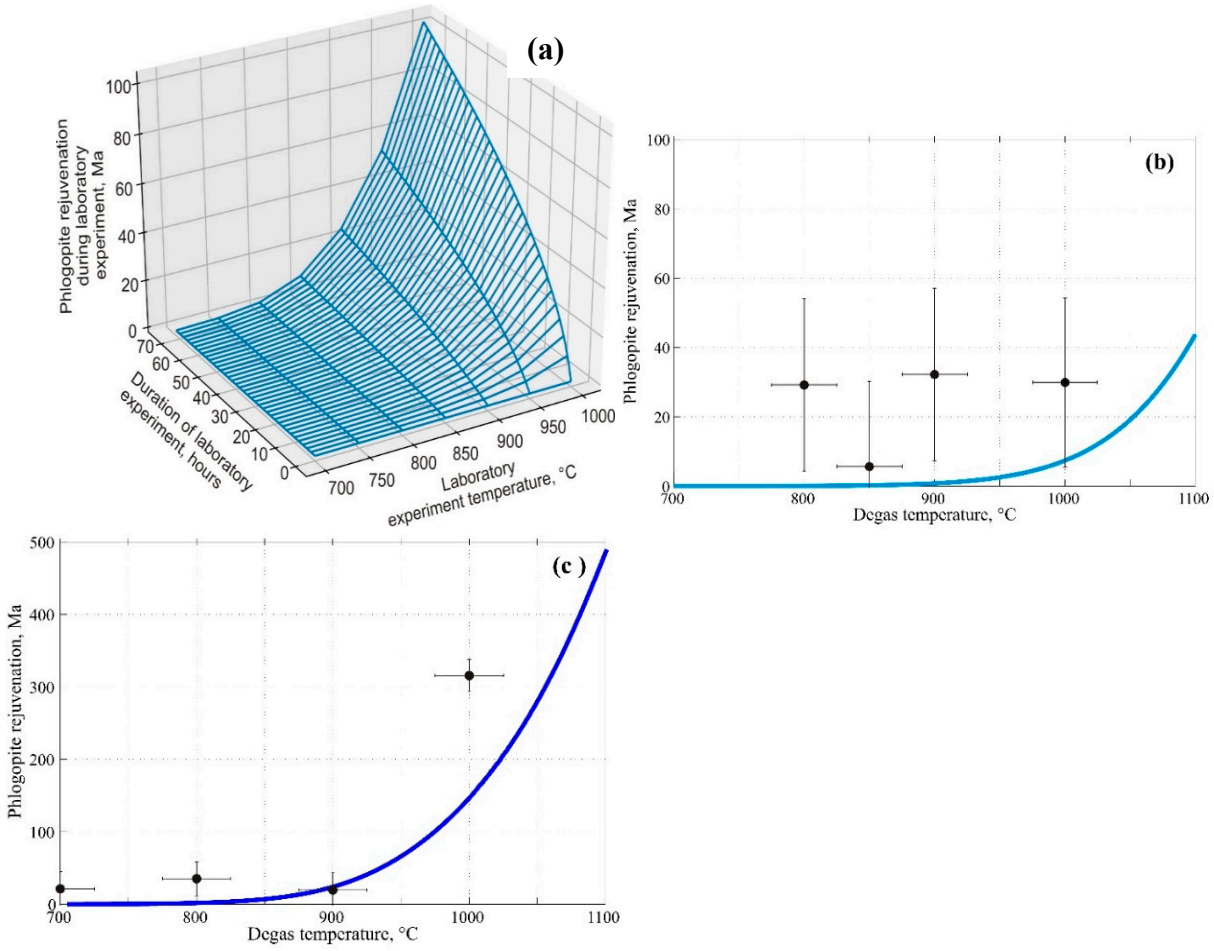

Figure 7. (**a**) Result of numerical modelling of evolution of the K/Ar isotopic system of phlogopite from magnesial skarns of the Aldanian shield (with 1902 Ma initial age) depending on conditions of the laboratory experiment (temperature and duration) at 3 GPa pressure. Rejuvenation degree of the isotopic system of phlogopite corresponds to the value in million years, by which its integral age decreased in the course of the experiment. Comparison between the results of laboratory experiments 2 h (**b**) and 72 h (**c**) long and the numerical simulation results.

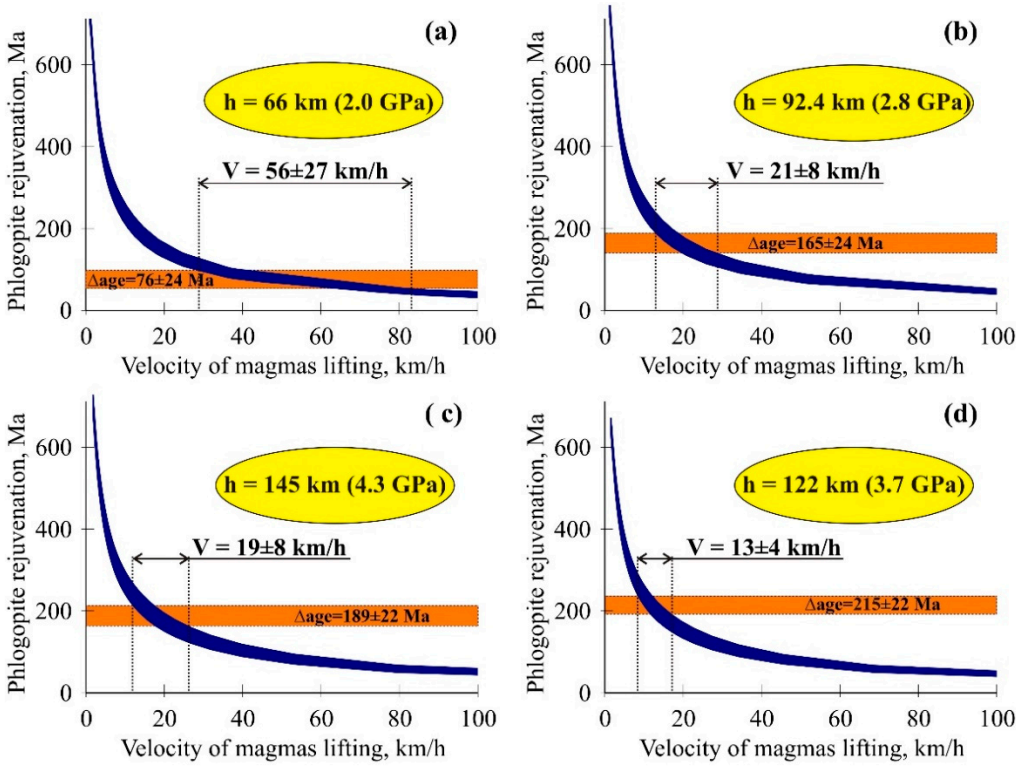

Figure 8. Result of numerical modelling of evolution of the K/Ar isotopic system of phlogopites from deep-seated xenoliths of kimberlite Mir (**a**) M5/01, (**b**) M4/01, (**c**) M31/01 and Udachnaya–Vostochnaya (**d**) UV300/09 pipes when rising to the Earth's surface.

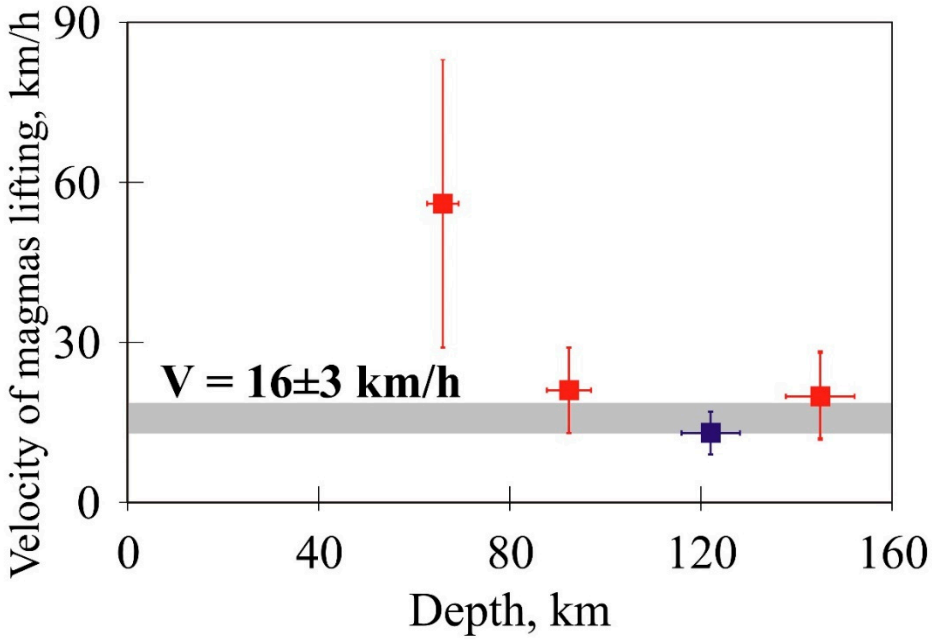

Figure 9. Estimate of the ascent rate of xenoliths in the kimberlite melt, based on the degree of radiogenic ^{40}Ar loss by phlogopite. Red colour—Mir pipe, blue colour—Udachnaya–Vostochnaya pipe.

6. Conclusions

Based on ^{40}Ar/^{39}Ar dating of phlogopite of mantle xenoliths of pyroxenites from diamond-bearing kimberlite Mir and Udachnaya–Vostochnaya pipes, we obtained the

estimates of age within 2568–2288 Ma, corresponding to the stage of early mantle metasomatism within the Siberian craton.

Laboratory experiments using phlogopite from magnesial skarns of the Aldanian shield (1872 Ma age) and Kuhi-Lal (Tajikistan, SW Pamir, 8.5 Ma age) and numerical simulation show that in conditions of increased P-T, the mobility of argon in the phlogopite lattice is in line with the concept of volume diffusion, and that, even in dry conditions, there is an efficient mechanism of exchange of radiogenic argon, released from the lattice of ancient phlogopite, with the structure of younger phlogopite. Thus, the survival of the mantle phlogopite isotopic system of metasomatic origin can be related to a limited volume of sinks for radiogenic ^{40}Ar, existing at depth.

The losses of radiogenic argon in phlogopite, when xenoliths of Mir, Udachnaya–Vostochnaya pipes rise to the surface in the kimberlite melt (temperature ~1000 °C), obtained through numeric simulation, and estimates of melting rate correlate with one another; the mean rate is 16 ± 3 km/h.

Author Contributions: D.Y. organized and coordinated experimental, 40Ar/39Ar studies, participated in the interpretation of the results and preparation of the article. N.M. conducted numerical simulations and participated in ^{40}Ar/^{39}Ar Dating. T.A. conducted selection, preparation, and research of a collection of deep xenoliths from kimberlite pipes. A.T. participated in ^{40}Ar/^{39}Ar Dating, interpretation of results, and preparation of the article. E.Z. conducted laboratory experiments with phlogopite under high P-T conditions. S.N. participated in the study of phlogopite samples before and after laboratory experiments. All authors have read and agreed to the published version of the manuscript.

Funding: The study was carried out within the framework of a State Assignment of Sobolev Institute of Geology and Mineralogy, Siberian Branch, Russian Academy of Sciences, Novosibirsk, under support of the Ministry of Science and Education of the Russian Federation, project no. 14.Y26.31.0012, and supported by the Russian Foundation for Basic Research no. 18-05-00211.

Acknowledgments: The authors are grateful to Alexey Ivanov for providing the Aldan phlogopite for laboratory research, and to Tatyana Smirnova for providing the phlogopite from the rocks of the Kuhi-Lal Deposit. Authors express sincere appreciation to Ludmila Pokhilenko for providing xenolith samples from Mir kimberlite, for her valuable comments and for a joint work on the earlier stages of this study.

Conflicts of Interest: The authors declare no conflict of interest.

References

1. Bulanova, G.P.; Muchemwa, E.; Pearson, D.G.; Griffin, B.J.; Kelley, S.P.; Klemme, S.; Smith, C.B. Syngenetic inclusions of yimengite in diamond from Sese kimberlite (Zimbabwe)—Evidence for metasomatic conditions of growth. *Lithos* **2004**, *77*, 181–192. [CrossRef]
2. Gregory, L.C.; Meert, J.G.; Pradhan, V.; Pandit, M.K.; Tamrat, E.; Malone, S.J. A paleomagnetic and geochronologic study of the Majhgawan kimberlite, India: Implications for the age of the Upper Vindhyan Supergroup. *Precambrian Res.* **2006**, *149*, 65–75. [CrossRef]
3. Phillips, D.; Harris, J.W. Provenance studies from ^{40}Ar/^{39}Ar dating of mineral inclusions in diamonds: Methodological tests on the Orapa kimberlite, Botswana. *Earth Planet. Sci. Lett.* **2008**, *274*, 169–178. [CrossRef]
4. Zaitsev, A.I.; Smelov, A.P. *Isotopic Geochronology of Rocks of the Kimberlite Formation of the Yakut Province*; IGABM SB RAS; Offset: Yakutsk, Russia, 2010; 108p.
5. Osborn, I.; Sherlock, S.; Anand, M.; Argles, T. New Ar–Ar ages of southern Indian kimberlites and a lamproite and their geochemical evolution. *Precambrian Res.* **2011**, *189*, 91–103. [CrossRef]
6. Kostrovitsky, S.I.; Solovyova, L.V.; Yakovlev, D.A.; Suvorova, L.F.; Sandimirova, G.P.; Travin, A.V.; Yudin, D.S. Kimberlites and megacrystal Association of minerals, isotope-geochemical studies. *Petrology* **2013**, *21*, 143–162. [CrossRef]
7. Pokhilenko, L.N.; Alifirova, T.A.; Yudin, D.S. ^{40}Ar/^{39}Ar-Dating of phlogopite from mantle xenoliths: Evidence of ancient deep metasomatism of the lithosphere of the Siberian craton. *Dokl. RAS* **2013**, *449*, 76–79. [CrossRef]
8. Yudin, D.S.; Tomilenko, A.A.; Travin, A.V.; Agashev, A.M.; Pokhilenko, N.P. Orihashi Yu. Age of introduction of the Udachnaya-Vostochnaya kimberlite pipe: U/Pb and ^{40}Ar/^{39}Ar data. *Dokl. RAS* **2014**, *455*, 91–93. [CrossRef]
9. Ashchepkov, I.V.; Logvinova, A.M.; Reimers, L.F.; Ntaflos, T.; Spetsius, Z.V.; Vladykin, N.V.; Downes, H.; Yudin, D.S.; Travin, A.V.; Makovchuk, I.V.; et al. The Sytykanskaya kimberlite pipe: Evidence from deep-seated xenoliths and xenocrysts for the evolution of the mantle beneath Alakit, Yakutia, Russia. *Geosci. Front.* **2015**, *6*, 687–714. [CrossRef]

10. Larionova, Y.O.; Sazonova, L.V.; Lebedeva, N.M.; Nosova, A.A.; Tretyachenko, V.V.; Travin, A.V.; Kargin, A.V.; Yudin, D.S. Age of the Arkhangelsk Province kimberlites: Rb-Sr, 40Ar/39Ar isotopic-geochronological and mineralogical data for phlogopite. *Petrology* **2016**, *24*, 607–639. [CrossRef]
11. Pushkarev, Y.D. *Actual Problems of K-Ar Geochronometry: Report at the 1st All-Union Workshop on Isotope Geochronology (5–12 May 1976)*; USSR AS. Geol. Inst. Kolsky Branch: Apatity, Russia, 1977; 54p.
12. Levskiy, L.K.; Levchenkov, O.A. *Geochronology and Geochemistry of Isotopes: Proceedings*; Pre-Cambrian Institute of Geology and Geochronology (USSR Academy of Sciences) Publ. House "Nauka", Leningrad Branch: Moscow, Russia, 1987; 216p.
13. Morozova, I.M.; Rublev, A.G. *Potassium-Argon Systems of Polymetamorphic Rocks*; Shukolyukov, Y.A.M., Ed.; Nauka: Moscow, Russia, 1987; pp. 19–28.
14. Lee, J.K.W. The argon release mechanisms of hornblende in vacuo. *Chemi. Geol.* **1993**, *106*, 133–160. [CrossRef]
15. Sletten, V.M.; Onstott, T.C. The effect of the instability of muscovite during in vacuo heating on 40Ar/39Ar step-heating spectra. *Geochim. Cosmochim. Acta* **1998**, *62*, 123–142. [CrossRef]
16. Lo, C.-H.; Lee, J.K.W.; Onstott, T.C. Argon release mechanisms of biotite in vacuo and the role of short-circuit diffusion and recoil. *Chem. Geol.* **2000**, *165*, 135–166. [CrossRef]
17. Lovera, O.M.; Grove, M.; Harrison, T.M.; Mahon, K.I. Systematic analysis of K-feldspar 40Ar/39Ar step heating results: I Significance of activation energy determinations. *Geochim. Cosmochim. Acta* **1997**, *61*, 3171–3192. [CrossRef]
18. Wartho, J.-A.; Kelley, S.P. 40Ar/39Ar ages in mantle xenolith phlogopites: Determining the ages of multiple lithospheric mantle events and diatreme ascent rates in southern Africa and Malaita, Solomon Islands. In *Geochronology: Linking the Isotopic Record with Petrology and Textures, Geological Journa*; Vance, D., Müller, W., Villa, I.M., Eds.; Special Publications: London, UK, 2003; Volume 220, pp. 231–248. [CrossRef]
19. Cassata, W.S.; Renne, P.R.; Shuster, D.L. Argon diffusion in plagioclase and implications for thermochronology: A case study from the Bushveld Complex, South Africa. *Geochim. Cosmochim. Acta* **2009**, *73*, 6600–6612. [CrossRef]
20. Hodges, K.V. Geochronology and Thermochronology in Orogenic Systems. In *Treatise on Geochemistry*; Elsevier: Oxford, UK, 2004; pp. 263–292. [CrossRef]
21. Lee, J.K.W.; Aldama, A.A. Multipath diffusion: A general numerical model. *Comput. Geosci.* **1992**, *18*, 531–555. [CrossRef]
22. Harrison, T.M.; Duncan, I.; McDougall, I. Diffusion of 40Ar in biotite—Temperature, pressure and compositional effects. *Geochim. Cosmochim. Acta* **1985**, *49*, 2461–2468. [CrossRef]
23. Harrison, T.M.; Celerier, J.; Aikman, A.B.; Hermann, J.; Heizler, M.T. Diffusion of 40Ar in muscovite. *Geochim. Cosmochim. Acta* **2009**, *73*, 1039–1051. [CrossRef]
24. Baxter, E.F. Diffusion of Noble Gases in Minerals. *Rev. Mineral. Geochem.* **2010**, *72*, 509–557. [CrossRef]
25. Kerchman, V.I.; Lobkovskiy, L.I. Specific features of geology, seismicity, and thermal behaviour of collision-zone belts, due to intracontinental subduction. *Rep. USSR Acad. Sci.* **1990**, 125–132.
26. Persikov, E.S.; Bukhtiyarov, P.G.; Sokol, A.G. Changes in viscosity of kimberlite and basaltic magmas in the processes of their origination and evolution (forecast). *Geol. Geophys.* **2015**, *56*, 1131–1140. [CrossRef]
27. Peslier, A.H.; Woodland, A.B.; Wolff, J.A. Fast kimberlite ascent rates estimated from hydrogen diffusion profiles in xenolithic mantle olivines from southern Africa. *Geochim. Cosmochim. Acta* **2008**, *72*, 2711–2722. [CrossRef]
28. Alifirova, T.A.; Pokhilenko, L.N. Features of microstructures and accessory mineralogy in garnet peridotites from the Udachnaya kimberlite pipe, Sakha Republic (Yakutia). Lithosphere and alkaline-ultramafic magmatism of the Siberian platform and its framing: Processes of formation of diamond deposits, methods of forecasting and prospecting. Collection of scientific papers on fundamental research of, V.S. Sobolev Institute of Geology and Mineralogy of the SB RAS. *Novosibirsk* **2018**, *2*, 4–16.
29. Pearson, D.G.; Kelly, S.P.; Pokhilenko, N.P.; Boyd, F.R. Laser 40Ar/39Ar analyses of phlogopites from Southern African and Siberian kimberlites and their xenoliths: Modelling of eruption ages, melt degassing, and mantle volatile compositions. *Geol. Geophys.* **1997**, *38*, 100–111.
30. Ichiro, K.; Ken-Ichiro, A. 40Ar/39Ar analyses of phlogopite nodules and phlogopite-bearing peridotites in South African kimberlites. *Earth Planet. Sci. Lett.* **1978**, *40*, 119–129. [CrossRef]
31. Phillips, D. Argon isotope and halogen chemistry of phlogopite from South African kimberlites: A combined step-heating, laser probe, electron microprobe and TEM study. *Chem. Geol. Isot. Geosci. Sect.* **1991**, *87*, 71–98. [CrossRef]
32. Hopp, J.; Trieloff, M.; Brey, G.P.; Woodland, A.B.; Simon, N.S.C.; Wijbrans, J.R.; Siebel, W.; Reitter, E. 40Ar/39Ar-ages of phlogopite in mantle xenoliths from South African kimberlites: Evidence for metasomatic mantle impregnation during the Kibaran orogenic cycle. *Lithos* **2008**, *106*, 351–364. [CrossRef]
33. Foland, K.A. Limited mobility of argon in a metamorphic terrain. *Geochim. Cosmochim. Acta* **1979**, *43*, 793–801. [CrossRef]
34. Roddick, J.C.; Cliff, R.A.; Rex, D.C. The evolution of excess argon in Alpine biotites. A 40Ar/39Ar analysis. *Earth Planet. Sci. Lett.* **1980**, *48*, 185–208. [CrossRef]
35. Dahl, P.S. The crystal-chemical basis for Ar retention in micas: Inferences from interlayer partitioning and implications for geochronology. *Contrib. Mineral. Petrol.* **1996**, *123*, 22–39. [CrossRef]
36. Smye, A.J.; Warren, C.J.; Bickle, M.J. The signature of devolatisation: Extraneous 40Ar systematics in high-pressure metamorphic rocks. *Geochim. Cosmochim. Acta* **2013**, *113*, 94–112. [CrossRef]
37. Baxter, E.F. Quantification of the factors controlling the presence of excess 40Ar or 4He. *Earth Planet. Sci. Lett.* **2003**, *216*, 619–634. [CrossRef]

38. Watson, E.B.; Baxter, E.F. Diffusion in solid-Earth systems. *Earth Planet. Sci. Lett.* **2007**, *253*, 307–327. [CrossRef]
39. Baksi, A.K.; Archibald, D.A.; Farrar, E. Intercalibration of 40Ar/39Ar dating standards. *Chem. Geol.* **1996**, *129*, 307–324. [CrossRef]
40. Chepurov, A.I.; Fedorov, I.I.; Sonin, V.M. Experimental study of diamond formation at high P-T parameters. *Geol. Geofiz.* **1998**, *39*, 234–244.
41. Zhimulev, E.I.; Chepurov, A.I.; Sonin, V.M.; Litasov, K.D.; Chepurov, A.A. Experimental modeling of percolation of molten iron through polycrystalline olivine matrix at 2.0–5.5 GPa and 1600 °C. *High Press. Res.* **2018**, *38*, 153–164. [CrossRef]
42. Chepurov, A.A.; Sonin, V.M.; Dereppe, J.M.; Zhimulev, E.I.; Chepurov, A.I. How do diamonds grow in metal melt together with silicate minerals? An experimental study of diamond morphology. *Eur. J. Mineral.* **2020**, *32*, 41–55. [CrossRef]
43. Davis, G.L.; Sobolev, N.V.; Khar'kiv, A.D. New data on the ageof Yakutian kimberlites obtained by the uranium-lead methodon zircons. *Dokl. Akad. Nauk SSSR* **1980**, *254*, 175–179.
44. Kinny, P.D.; Griffin, B.J.; Heaman, L.M.; Brakhfogel, F.F.; Spetsius, Z.V. SHRIMP U-Pb ages of perovskite from Yakutian kimberlites. *Geol. Geofiz.* **1997**, *38*, 91–99.
45. Winterburn, P.A.; Harte, B.; Gurney, J.J. Peridotite xenoliths from the Jagersfontein kimberlite pipe: I. Primary and primary metasomatic mineralogy. *Geochim. Cosmochim. Acta* **1990**, *54*, 329–341. [CrossRef]
46. Erlank, A.J.; Water, F.G.; Haggerty, S.E.; Hawkesworth, C.J. Characterization of metasomatic processes in peridotite nodules contained in kimberlite. In Proceedings of the 4th International Kimberlite Conference: Extended Abstracts, Perth, Australia, 11–15 August 1986; pp. 232–234.
47. Solovieva, L.V.; Vladimirov, V.M.; Dneprovskaya, L.V.; Maslovskaya, M.I.; Brandt, S.B. *Kimberlites and Kimberlite-Like Rocks: Upper Mantle Material under Ancient Platforms*; VO "Nauka": Novosibirsk, Russia, 1997; 256p.
48. Galimov, E.M.; Solovieva, L.V.; Belomestnykh, A.V. Isotopic composition of carbon from metasomatically altered mantle rocks. *Geochemistry/Geokhimiya* **1989**, *4*, 508–515.
49. Rozen, O.M.; Manakov, A.V.; Serenko, V.P. Palaeoproterozoic collision system and diamond-bearing crustal root of the Yakutsk kimberlite province. *Geol. Geophys.* **2005**, *46*, 1259–1272.
50. Nimis, P.; Taylor, W.R. Single Clinopyroxene Thermobarometery for Garnet Peridotites. Part, I. Calibration and Testing of the Cr-in-Cpx Barometer and an Enstitite-in-Cpx Thermometer. *Contrib. Mineral. Petrol.* **2000**, *139*, 541–554. [CrossRef]
51. Brey, G.P.; Köhler, T. Geothermobarometry in Four-phase Lherzolites II. New Thermobarometers, and Practical Assessment of Existing Thermobarometers. *J. Petrol.* **1990**, *31*, 1353–1378. [CrossRef]
52. Tutti, F.; Dubrovinsky, L.S.; Saxena, S.K. High pressure transformation of jadeite and stability of NaAlSiO4 with calcium-ferrite type structure in the lower mantle conditions. *Geophys. Res. Lett.* **2000**, *27*, 2025–2028. [CrossRef]
53. Tutti, F.; Lazor, P. Temperature-induced phase transition in phlogopite revealed by Raman spectroscopy. *J. Phys. Chem. Solids* **2008**, *69*, 2535–2539. [CrossRef]
54. Comodi, P.; Fumagalli, P.; Montagnoli, M.; Zanazzi, P.F. A single-crystal study on the pressure behavior of phlogopite and petrological implications. *Am. Mineral.* **2004**, *89*, 647–653. [CrossRef]
55. Chon, C.-M.; Lee, C.-K.; Song, Y.; Kim, S.A. Structural changes and oxidation of ferroan phlogopite with increasing temperature: In situ neutron neutron powder diffraction and Fourier transform infrared spectroscopy. *Phys. Chem. Miner.* **2006**, *33*, 289–299. [CrossRef]
56. Giletti, B.J. Studies in diffusion. Argon in phlogopite mica. In *Geochemical Transport and Kinetics. Carnegie Institution of Washington*; Hofmann, A.W., Giletti, B.J., Yoder, H.S., Jr., Yund, R.A., Eds.; Carnegie Institution of Washington: Washington, DC, USA, 1974; pp. 107–115.
57. Hodges, K.V.; Hames, W.E.; Bowring, S.A. 40Ar/39Ar gradients in micas from a high-temperature-low-pressure metamorphic terrain: Evidence for very slow cooling and implications for the interpretation of age spectra. *Geology* **1994**, *22*, 55–58. [CrossRef]
58. Giletti, B.J.; Tullis, J. Studies in diffusion. Pressure dependence of Ar Diffusion in Phlogopite mica. *Earth Planet. Sci. Lett.* **1977**, *35*, 180–183. [CrossRef]
59. McDougall, I.; Harrison, T.M. *Geochronology and Thermochronology by the 40Ar/39Ar Method*; Oxford University Press: Oxford, UK, 1999.
60. Lister, G.S.; Baldwin, S.L. Modelling the effect of arbitrary P-T-t histories on argon diffusion in minerals using the MacArgon program for the Apple Macintosh. *Tectonophysics* **1996**, *253*, 83–109. [CrossRef]